Comparing Battery Solutions for Intercity In–Motion Charging Buses

An Arnhem-Wageningen Case Study

Mirza Khalid Baig

TU Delft

Comparing Battery Solutions for Intercity In–Motion Charging Buses

An Arnhem-Wageningen Case Study

Thesis report

by

Mirza Khalid Baig

to obtain the degree of Master of Science
at the Delft University of Technology
to be defended publicly on September 29th, 2023 at 10:30

Thesis committee:

Chair:	Prof. Dr. ir. Pavol Bauer
Supervisors:	Dr. ir. Gautham Ram Chandra Mouli
	Dr. ir. Dennis van der Born
PhD Supervisor:	Ibrahim Diab
Place:	Faculty of EEMCS, Delft
Project Duration:	November 14th, 2022 - September 29, 2023
Student number:	5532736

An electronic version of this thesis is available at `http://repository.tudelft.nl/`.

Faculty of EEMCS · Delft University of Technology

Preface

In the course of my Bachelor's degree in Mechanical Engineering in India, I had the privilege of joining a Formula Student team. It was during this period that I was first introduced to the intricacies of electric vehicles, igniting a profound interest in this domain. As my final year approached, I made a decisive commitment to pursue a Master's degree in Sustainability with a dedicated focus on clean energy.

Upon commencing my Master's studies at Delft, I was drawn to the Electric Mobility Systems cluster, fueled by a passion to delve deeper into the realm of electric vehicle technologies. Several coursework experiences, particularly those related to batteries, played a pivotal role in shaping my academic journey and ultimately led to the selection of my thesis topic. My choice to explore the concept of intercity IMC buses was driven by its potential for sustainable urban transportation.

I extend my heartfelt gratitude to Dr. Gautham for his invaluable guidance and support during the entirety of my thesis journey. I also wish to express my sincere appreciation to Prof. Dr. Ir. Bauer and Dr. Ir. Dennis van der Born for graciously being on my thesis committee. A special note of appreciation goes to Ibrahim, whose mentorship and constructive feedback have been instrumental in shaping this thesis. I am grateful for his continuous support and mentorship.

Additionally, I extend my gratitude to my friends in Delft, whose encouragement has been a constant source of motivation. Above all, I owe an immeasurable debt of thanks to my family, and their unwavering support, without which this academic milestone would not have been possible.

Mirza Khalid Baig

Delft, September 2023

Abstract

The emergence of electric mobility in urban public transportation, with a particular focus on electric buses, presents a promising solution to address emissions and environmental concerns. However, a significant challenge lies in ensuring continuous bus operation without the need for frequent charging. In-motion charging (IMC), often referred to as dynamic charging, is a concept engineered to overcome this challenge. IMC technology empowers electric buses to charge during motion, combining the advantages of both trolleybuses and battery electric buses.

A comprehensive study was undertaken to know the potential and practicality of intercity IMC buses. A bus model was developed to assess the power traction capabilities of these vehicles. This model served as the foundation for exploring four distinct charging scenarios, each characterized by varying charging powers and strategies.

An investigation into the unique battery load profiles observed in intercity IMC buses across the different charging scenarios was done. This was essential for understanding the intricacies of power demand, especially in scenarios where the bus relies heavily on catenary charging. Notably, the introduction of in-motion charging in the first scenario (IMC only) underscored the critical role of catenary charging power in meeting operational demands. Subsequent integration of a stationary charging system at Arnhem Central showcased the potential to reduce catenary charging power, offering prospects for enhancing battery health.

The second part of the thesis delved into the comparative effect of various charging scenarios on the aging of commonly employed battery chemistries in IMC vehicles. Using comprehensive battery models, the aging dynamics under diverse conditions were studied. It became evident that each scenario held distinct implications for battery aging.

Lastly, the study addressed the pivotal question of cost-effective battery selection for intercity IMC buses. An exploration of four distinct scenarios, in conjunction with different battery chemistries, yielded valuable insights into their respective performances. Lithium-titanate (LTO) batteries consistently emerged as the preferred choice. Their extended lifespan, reduced replacement frequency, and overall cost-effectiveness positioned them as the frontrunners in the context of intercity IMC bus systems. This consensus held across most scenarios, underscoring the practicality of LTO batteries.

In conclusion, the transportation sector's substantial impact on greenhouse gas emissions and urban air quality necessitates innovative and sustainable solutions. Intercity IMC buses, along with optimal battery selection and charging strategies, represent a promising avenue for sustainable urban transportation. Among battery chemistries, LTO batteries have proven to be the most cost-effective choice for powering intercity IMC bus operations.

Contents

List of Figures

List of Tables

1 Introduction

This chapter serves as an introduction to the necessity of in-motion charging (IMC) buses, positioning them as a prospective solution for clean public transportation systems. Various IMC bus projects encompassed within the Trolley 2.0 initiative are explained. Furthermore, this chapter sheds light on the central research questions that this thesis addresses. Lastly, an outline of the thesis structure is presented, to guide the reader through the subsequent chapters.

1.1. Electric Transportation

The transportation sector is a significant contributor to greenhouse gas emissions in the European Union (EU). In fact, almost one-fourth of the EU's greenhouse gas emissions are attributable to transportation, which is also the primary source of air pollution in urban areas. Urban mobility is responsible for approximately 40% of all CO2 emissions from roads [1, 2]. In order to address the threat that climate change poses to urban areas, it is extremely important to ensure a low-carbon transportation sector. Transportation and mobility play a crucial role in both urban economics and quality of life.

The vast majority of buses in Europe are currently reliant on diesel fuel, thereby contributing to the release of greenhouse gases and other harmful pollutants. In order to mitigate these negative environmental impacts, there is an urgent need to develop more sustainable and eco-friendly alternatives. This is especially crucial since urban public transportation vehicles are typically operational for up to 16 hours per day, and thus have a significant impact on emissions in urban areas [3].

Electric vehicles are often viewed as a potential solution to the problem of greenhouse gas emissions from conventional vehicles, given their lack of tailpipe emissions [4]. A study by [5] demonstrated that while the addition of more electrified bus routes to the bus network could potentially reduce emissions, it does not always lead to an overall decrease in emissions. The study identified electric buses with 120 kWh batteries as having the lowest life cycle emissions. Therefore, when implementing electric mobility solutions, careful consideration of battery size and technology is required to ensure environmental benefits.

However, implementing electric vehicles for public transport is not a straightforward process and is faced with several complications.

- **Driving range**: The limited driving range is a significant challenge for the implementation of electric vehicles in public transport systems. Although this issue is being continuously addressed, it remains a concern.
- **Charging time**: The charging time of battery packs for electric vehicles is a major concern, as it can significantly impact the operation and productivity of the vehicle. While the battery pack can take 4 to 8 hours to fully charge, "fast charging" technology can charge the battery to 80% of its capacity in as little as 30 minutes. For example, Tesla superchargers can charge the Model S to 50% or 80% of its capacity in just 20 or 30 minutes, respectively [4]. However, the availability and infrastructure of fast charging stations are still limited in many regions.
- **Battery cost**: Large battery packs are typically expensive, which can significantly increase the overall cost of an electric vehicle, especially for public transportation where numerous vehicles are required.

- **Bulk and weight**: The size and weight of battery packs are significant, which can pose challenges in terms of accommodating them in vehicles.

In light of these challenges, there is ongoing research into a novel form of public transportation that employs dynamic charging, aiming to establish a practical solution for widespread adoption within the public transport sector.

1.2. In-motion Charging

Electric mobility has become an increasingly important topic in public transportation, particularly in urban areas. Battery electric buses, propelled by electric motors drawing power from batteries have become more prevalent, and advancements in electrochemical battery technology have improved their capabilities. However, the use of electric buses for continuous urban transportation without the need for frequent charging is currently not feasible [6].

Another form of electric bus is the trolleybus, which draws power from a trolley-grid infrastructure for traction and represents a fully electric urban transportation mode while mitigating environmental concerns by producing zero tailpipe emissions [4]. Despite their eco-friendly advantages, trolleybuses have face operational limitations due to fixed routes. Some trolleybuses were equipped with small batteries to provide short-distance electric traction, enhancing safety during network failures. Recent advancements in battery technology have ushered in a new era for these vehicles, enabling extended autonomous journeys and prompting initiatives like ”Trolley 2.0” in Europe [7]. This evolution has catalyzed the adoption of in-motion charging (IMC) bus pilot projects in various European cities, as detailed in the examples discussed in the subsequent sections (see Section 1.3).

In-motion charging, also known as dynamic charging, is a concept that has been developed to address challenges faced by battery electric buses and trolleybuses. This technology enables electric buses to operate for significant stretches in battery mode, combining the benefits of both trolleybuses and battery electric buses. This results in a significant reduction in the number of installed catenary wires [8]. The IMC system operates by using overhead cables at the first segment as a power source for traction and to charge the onboard storage. The remainder of the route is devoid of contact points with the trolley grid. In the later section, the vehicle operates independently on the catenary and is propelled by the battery [6, 8].

Overall, there is a lot of potential for in-motion charging technology to increase the viability of electric buses for urban transportation. It combines the benefits of both e-buses and trolleybuses and the need for catenary wires is lessened, making it a more practical choice for cities looking to switch to sustainable public transportation.

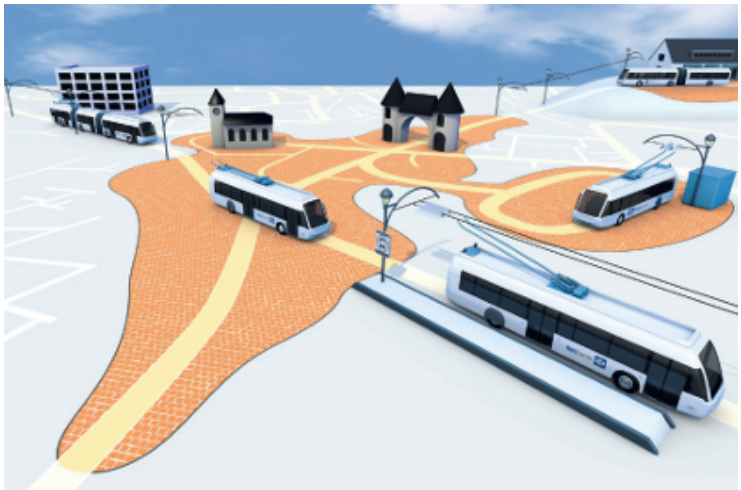

Figure 1.1: In-motion charging system [9]

1.3. Range in IMC buses

Over the past few years, several IMC bus pilot projects have been implemented in Europe. These projects are aimed at exploring the feasibility of battery-electric trolley buses and the benefits they can achieve through in-motion charging technologies. One such project is the trolley:2.0 initiative supported by Electric Mobility Europe (EMEurope) [7].

- Praha, Czech Republic: A shortened route of 5 km from Palmovka to Letany, with electric buses operating on the IMC system, was approved in 2017. 20% of the test route's total length, or one kilometer, between the Kundratka and Kelerka stops, consisted of a dedicated trolleybus overhead catenary. Other IMC projects include a route that is 10% catenary-covered over a distance of 10 km [9].
- Szeged, Hungary: To replace diesel buses with hybrid trolleybuses, Szegedi Közlekedési Kft (SZKT) used 13 articulated IKARUSSKODA trolleybuses with 80 kWh capacity batteries. The IKARUS-SKODA trolleybuses replaced the buses on SZKT's route 77A with a total distance of 13.2 km with more than 50% of the route run on battery mode. In April 2020, an 8 m trolleybus was designed and tested which is planned to run on the 77A line in Szeged, where it will travel up to 20 km without an overhead line over a 30-kilometer stretch [7].
- Marrakesh, Morocco: A bus line with a total length of 8 km that runs through Hassan II Avenue and links the city's center with its western suburbs was inaugurated in September 2017. Around 30% of the total length is the catenary-covered section [10].
- Gyndia, Poland: One of the first in Europe, PKT Gdynia started operating trolleybuses with an In Motion Charging system in 2009. The buses have high-capacity lithium-ion batteries with capacities of 40 kWh and 69 kWh that can travel up to 12 km, with battery mode accounting for 85% of that distance [10].
- Solingen, Germany: Since 2018, Solingen has operated four electric articulated buses equipped with IMC500 technology. They are known as BOBs (battery overhead wire buses) in Solingen and currently travel 75% of the distance on 12 km of overhead wire sections [11]. Another route in Solingen makes use of IMC500 buses, which can run wirelessly at close to 80% of their capacity over an 18-kilometer roundtrip when charged back and forth [9].
- Eberswalde, Germany: Lithium-ion batteries are installed in buses from BBG Eberswalde. The regional bus line, which is currently powered by diesel engines, will be entirely converted by BBG so that it can run on battery power. It will travel a total of 23 km with a 6.5 km catenary length.
- Arnhem, Netherlands: a pioneering IMC trolley bus system is to be deployed for intercity travel between Arnhem Central and Wageningen, spanning approximately 35 kilometers for a complete roundtrip. Notably, there exists just one catenary system in Arnhem, extending roughly 4.3 kilometers from the city center to Oosterbeek.

A majority of initial pilot projects have primarily focused on shorter routes, employing smaller battery capacities to accommodate the limited distances necessitated by battery mode operation. Consequently, these initiatives have managed to operate with minimal Depth of Discharge (DoD) levels. However, the Arnhem case presents a distinctive contrast within this landscape. Spanning a battery mode operation covering 26 kilometers, this project demands a considerably larger battery capacity in comparison to its counterparts.

The aging dynamics of batteries employed in intracity bus projects remain relatively unexplored, largely due to their shallow cycle patterns and operation within safe State of Charge (SOC) thresholds. Yet, the scenario undergoes a significant shift when considering inter-city travel. Maintaining shallow cycles and adhering to restricted SOC limits necessitates a substantially larger battery capacity similar to that of electric buses. In such instances, the feasibility of IMC buses as a concept may diminish. As a result, a compelling need arises to meticulously examine intercity travel within the framework of IMC buses.

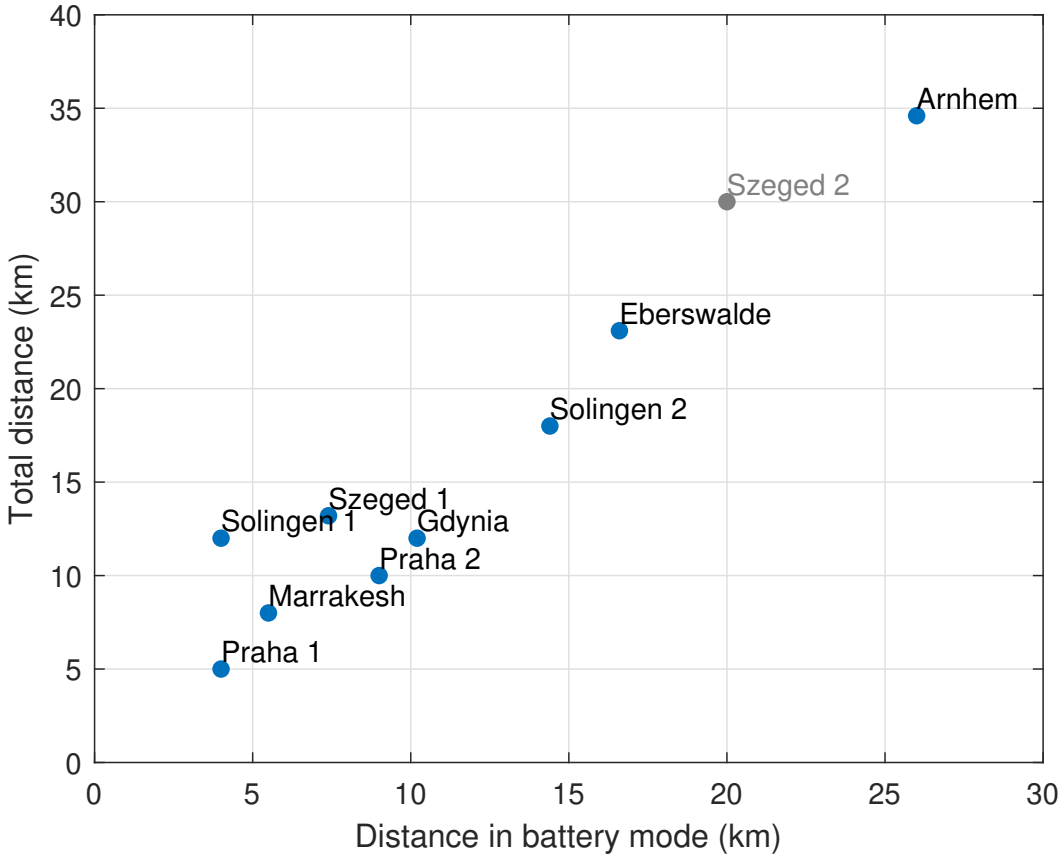

Figure 1.2: IMC Projects: Total distance of a trip to distance in battery mode

1.4. Research Formulation

The formulation of the research questions is aimed at addressing particular gaps in current knowledge and exploring key challenges and considerations in the domain of IMC buses for intercity travel. These questions seek insights that will facilitate the advancement in the implementation of IMC buses in the context of intercity travel.

Research Question 1

How can distinct battery load profiles be developed in inter-city IMC buses for varying charging scenarios?

This question aims to understand how different charging scenarios impact the battery load profiles in inter-city IMC buses. To construct these load profiles, the initial step involves comprehensively calculating the power and energy requisites for intercity IMC buses across a year of operation, accounting for seasonal fluctuations. Different charging scenarios are considered, encompassing various combinations of IMC with opportunity charging and depot overnight charging. Since these buses cover longer distances, the varying charging conditions can lead to different load distributions on the battery. This knowledge is crucial to predict potential impacts on battery lifespan. By considering different load profiles, the aim is to identify the best charging scenario.

Research Question 2

What is the comparative effect of various charging scenarios on the aging of commonly employed battery chemistries in IMC vehicles?

This question delves into the relationship between charging scenarios and battery aging. Battery aging is a critical factor in determining the longevity of batteries. By comparing the effects of different charging scenarios on commonly used battery chemistries, one can gauge which scenarios lead to accelerated or mitigated battery aging. To achieve this, the utilization of semi-empirical models from existing literature emerges as a viable approach to gain insights into the aging of different battery chemistries.

Research Question 3

How do different traction battery solutions compare in the context of inter-city IMC buses?

Given the larger distances covered by inter-city buses, finding the right battery type and size is crucial to strike a balance between the cost and performance of the battery. This question underscores the need to identify batteries that can withstand the demands of inter-city travel while being economically viable. It involves evaluating factors such as battery characteristics, weight, and replacement costs of different battery chemistries.

1.5. Structure of the Report

This master's thesis follows the following structure

- **Chapter 1 - Introduction**
  This section comprises an introduction to the concept of in-motion charging, IMC pilot projects, and outlines the research objectives of the thesis.

- **Chapter 2 - Literature Review**
  In this chapter, a comprehensive review of relevant literature is presented, encompassing subjects such as in-motion charging bus requirements, battery technology, battery aging, and battery models.

- **Chapter 3 - Development of Battery Load Profiles**
  Within this chapter, different charging scenarios are explained, followed by the formulation of a battery load profile for each specific scenario.

- **Chapter 4 - Battery Aging**
  This chapter includes the aging of different battery chemistries under different charging scenarios using aging models.

- **Chapter 5 - Battery Size Optimization**
  In this chapter, optimal battery sizes are determined through an optimization process that incorporates insights from the aging results.

- **Chapter 6 - Conclusion**
  This chapter contains the conclusion and offers recommendations for future work.

2

Literature Review

The primary objective of this chapter is to conduct a literature review on IMC systems and identify any gaps in the existing knowledge. Section 2.1 delves into trolleybuses and the concept of IMC, and section 2.2 and 2.3 discusses the battery requirements and battery chemistries with a particular focus on the IMC bus. Battery aging and modeling literature are discussed in Section 2.4. Section 2.5 discusses the financial aspects of IMC bus projects. Finally, the research gaps are presented in Section 2.6.

2.1. Trolleybus and in-motion charging bus

Trolleybuses, although in use since the early 20th century, faced a decline in popularity during the mid-20th century due to operational constraints and the emergence of more cost-effective diesel buses. However, the energy crisis of the 1970s, marked by escalating oil prices, led to a resurgence of interest in trolleybuses [12]. This renewed attention prompted the reinstallation of trolleybus systems in various countries globally. In the contemporary era, numerous cities worldwide, such as Salzburg in Austria, Gdynia in Poland, and Arnhem in the Netherlands, have adopted trolleybuses as a significant component of their urban transportation networks [7].

Trolleybuses are propelled by an electric motor, which is powered by a trolley-grid infrastructure. This trolley-grid system not only furnishes power for the trolleybus's movement but also caters to its auxiliary power needs, making the trolleybus an entirely electric mode of urban transportation. Unlike the buses relying on gasoline-based fuels, trolleybuses produce no tailpipe emissions, aligning with the growing environmental consciousness [4].

While trolleybuses offer reduced pollution, they are not without operational limitations. In the past, certain trolleybuses were equipped with small batteries, enabling them to operate over short distances with access to electric traction. This feature added a safety buffer in urban traffic during network failures. However, the recent advancements in battery technology have spurred the evolution of these vehicles toward extended journeys in an autonomous mode. Trolley 2.0 is one initiative taken by the European countries to adopt new and improved versions of trolleybus [7]. This evolution has paved the way for the implementation of in-motion charging (IMC) bus pilot projects in numerous European cities, which were elaborated in Section 1.3.

A comparative illustration of IMC bus in contrast to a standard electric bus is provided in Figure 2.1. The standard electric bus typically recharges at designated stations, either overnight or through opportunity charging, and subsequently operates the entire route in battery mode. This approach results in prolonged charging times and necessitates a larger battery size to accommodate the entire operational route. In contrast, the IMC bus charges while in motion under the catenary, subsequently transitioning to battery mode for the remaining route. This eliminates the need for stationary charging pauses and, significantly, leads to a reduction in battery size i comparison to a battery electric bus.

To elucidate this with a numerical example, let's consider an energy requirement of 2 kWh per kilometer and a total distance of travel to be 10 km. In the case of a standard electric bus operating at a DoD of 50%, it would necessitate a 40 kWh battery to cover its operational needs. Furthermore, extended charging times at stations would be required. On the other hand, an IMC bus, covering 7 km in battery mode, would

suffice with a smaller 28 kWh battery to meet the same operational demands at a 50% DoD. This smaller battery also benefits from charging during the 3 km span under the catenary, eliminating the requirement for stationary charging at terminals. Additionally, owing to its capability to operate in battery mode, the IMC bus can also navigate routes that lack a trolley-grid infrastructure. Thus, the IMC bus combines the advantages of both a conventional electric bus and a traditional trolleybus.

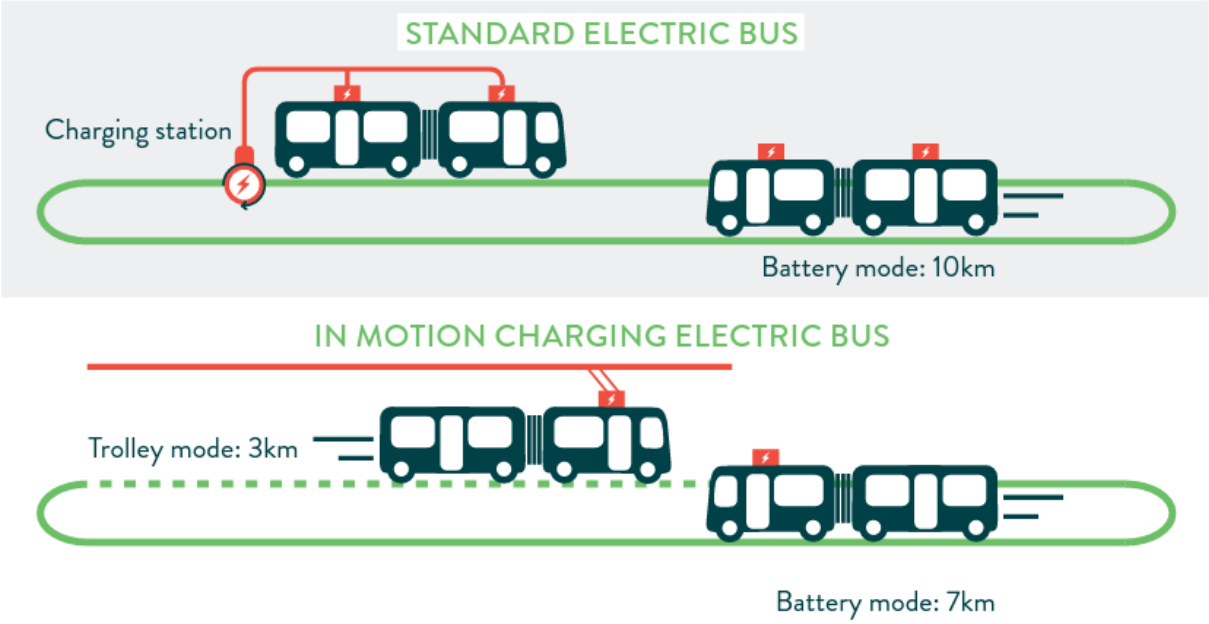

Figure 2.1: An example of the standard (battery) electric bus to an IMC bus [13]

2.2. Charging under the trolleygrid

The charging of the battery under the catenary can be realized through different approaches, each offering distinct strategies for managing the battery charging power.

- Conventional IMC charging (regular charging): Conventional IMC charging, also known as regular charging, involves maintaining a constant battery charging power at all trolley grid substations. Regardless of the specific substation location, the battery charging power remains unchanged. This approach ensures a consistent and predictable charging process for the trolleybus grid system, simplifying the implementation and management of the charging infrastructure [14].
- Adaptive charging: Adaptive charging represents an alternative approach where the battery charging power is dynamically adjusted based on the specific trolleygrid substation where the bus is located. The charging power varies depending on the substation's characteristics and power availability. This adaptive strategy optimizes the charging process to match the conditions at each substation, potentially improving resource utilization [14].
- Valley charging: Valley charging is another charging method found in the literature. It involves the battery charging power adjusting while the bus travels under a substation, depending on the current state of the trolleygrid. During periods of lower electricity demand (valley periods), the charging power may be increased to capitalize on excess power availability and charge the battery more rapidly. Conversely, during peak demand times, the charging power may be reduced to avoid adding strain to the electrical grid [15].

2.3. Battery requirements

The cycle lifetime of the battery is a critical requirement for the IMC bus, given its constant charge and discharge cycles during its daily commute. To meet the charging corridor length constraints, it is essential to

maintain a continuous power density that enables fast charging, which is necessary for IMC bus operation.

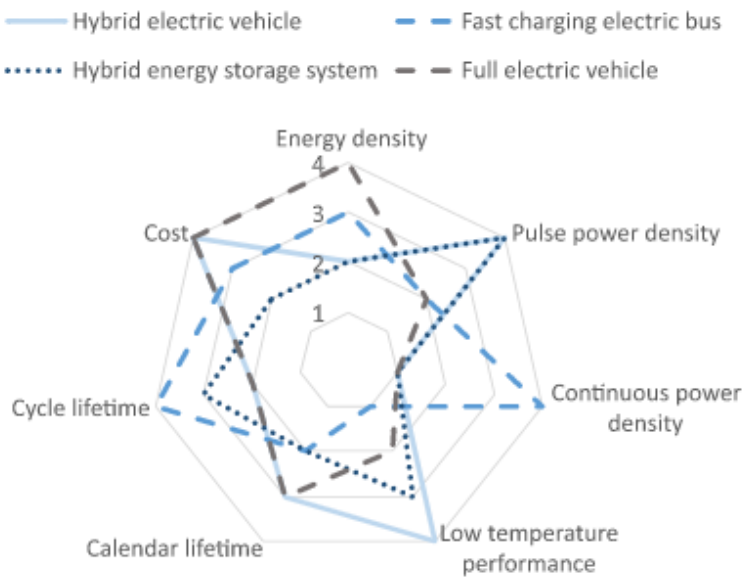

Figure 2.2: Battery cell specifications for use in various automotive applications (1: low significance, 4: high significance) [16]

Battery technology can be categorized using a number of factors. The following describes the most crucial parameters:

- Energy Density: Energy density refers to the battery's ability to store a high amount of energy within a smaller mass, which is crucial for achieving a longer range for the vehicle. As depicted in Figure 2.3, Li-ion batteries are a promising choice for electric vehicle applications, as they offer high energy density at varying power densities compared to other storage options. The figure shows the energy density of various storage options, emphasizing the advantageous position of Li-ion batteries in terms of energy density for EV use.
- Power Density: A battery system with high power density can deliver large amounts of energy output based on its mass. The power density of a battery system is closely associated with its ability to fast charge, which is of paramount importance for IMC buses. A higher power density implies that the battery can charge faster, which is essential given the time constraints imposed by the charging corridor limits. Thus, the charging power must be high to minimize charging time, as highlighted in [6].
- Cycle life: The battery's cycle lifetime refers to the number of cycles it can undergo before experiencing failure. The cycle life is typically defined as the number of times a battery can be discharged before it can only store 80% of its original energy capacity, as reported in [18]. The depth of discharge, C-rate, and average SOC are factors that can impact the length of a cycle. For an IMC bus, cycle lifetime is a critical parameter, as the battery represents a significant portion of the vehicle's cost. Therefore, selecting a battery with a longer cycle life is advantageous, given other factors.
- Depth of Discharge: The depth of discharge is an essential factor affecting the cycle life of batteries, as it determines the percentage of energy capacity utilized during each discharge cycle [18]. Studies have shown that using a battery at 50% DoD instead of 100% DoD can increase the cycle life by almost three times [18]. However, the impact of DoD on cycle life can vary significantly depending on the battery chemistry and system. In the case of an IMC bus, the weight of the battery system can be influenced by DoD. A lighter battery system can be achieved by using a battery with a 100 kWh capacity at 100% DoD compared to a 200 kWh capacity battery at 50% DoD. To enhance the cycle life of battery systems, a lower DoD than 100% is sometimes used. However, LTO batteries are one battery chemistry that can operate with high DoDs, making them a potential option for IMC buses [19].
- Calender lifetime: The calendar life of a battery refers to the duration during which it can remain inactive or have minimal use while maintaining at least 80% of its initial capacity. High temperatures

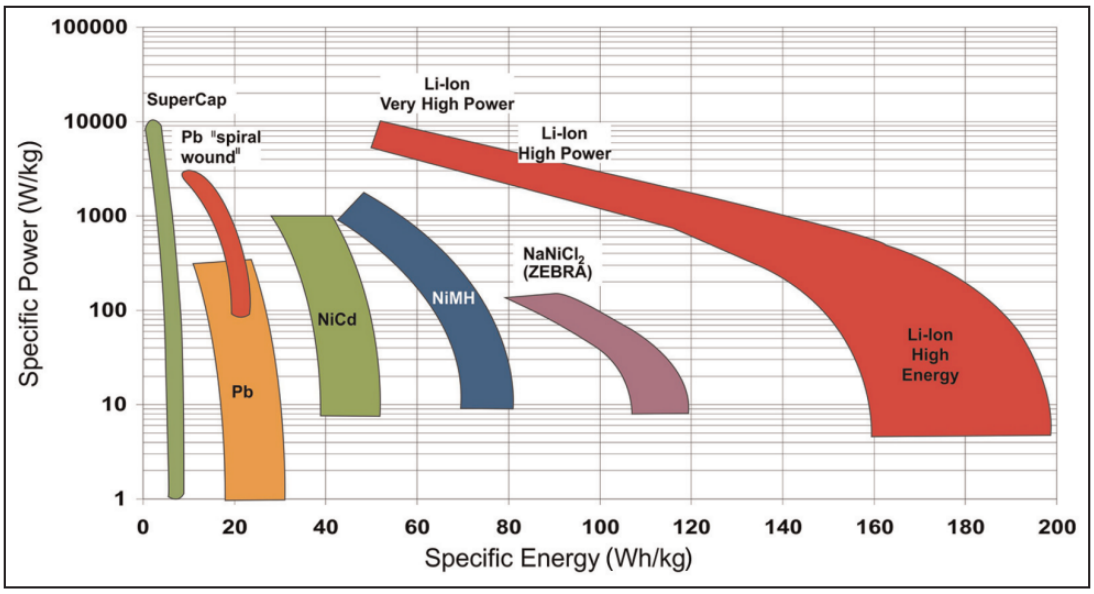

Figure 2.3: Ragone plot showing a variety of storage technologies for automotive applications [17]

accelerate the aging process of the battery. Therefore, many high-performance batteries in regular vehicles tend to deteriorate prematurely due to calendrical aging, rather than capacity turnover [17].

- Effective lifecycle cost: Due to the limited lifespan of batteries, their price can be standardized to cost per kWh per cycle depending on how many discharge cycles they can withstand. [18] provides an equation that can be used to calculate the effective life cycle cost of a battery:

$$\text{Effective Life Cycle Cost} = \frac{\text{Battery cost per kWh of storage}}{\text{Cycle Life}} \tag{2.1}$$

This equation is used to determine the most cost-effective battery for a given application. For example, a battery with a lower upfront cost but a shorter cycle life may have a higher effective life cycle cost than a more expensive battery with a longer cycle life. This calculation is essential in the selection of batteries for IMC buses, as their battery packs account for a significant portion of the vehicle's cost.

2.4. Batteries for IMC buses

A battery is made up of cells, each of which has an anode, a cathode, and an electrolyte between the two electrodes. For Li-ion cells, many materials, such as transition metal oxides (lithium cobalt oxide, lithium manganese oxide, nickel cobalt aluminum oxide, nickel manganese cobalt oxide) or phosphates (lithium iron phosphate, or LFP), have become common for the cathode of a Li-ion battery cell because of their high redox potentials versus Li/Li+ [16].

2.4.1. Graphite-anode based batteries

Graphite serves as a prevalent anode material in numerous commercial applications owing to its lower redox potential in comparison to Li/Li+. Its structure comprises parallel graphene layers that are arranged with a certain degree of shift relative to each other. During the process of lithium-ion insertion into this structure, the spaces between these layers expand to accommodate the lithium ions. As a result, lithiation leads to an approximate 10% expansion in the volume of the graphite material [20]. Regarding IMC buses, the commonly employed battery configuration incorporates graphite anode alongside cathode materials such as LFP and NMC [21].

2.4.2. LTO-anode based battery

Because of its appealing battery performance in rate characteristics and chemical stability, the lithium titanate battery—which uses $Li_4Ti_5O_{12}$ (LTO) as its anode rather than graphite—has emerged as a leading candidate for fast charging and power assist vehicular applications [22]. Figure 2.4 compares the performance characteristics of an LTO with graphite as an anode of a Li-ion cell.

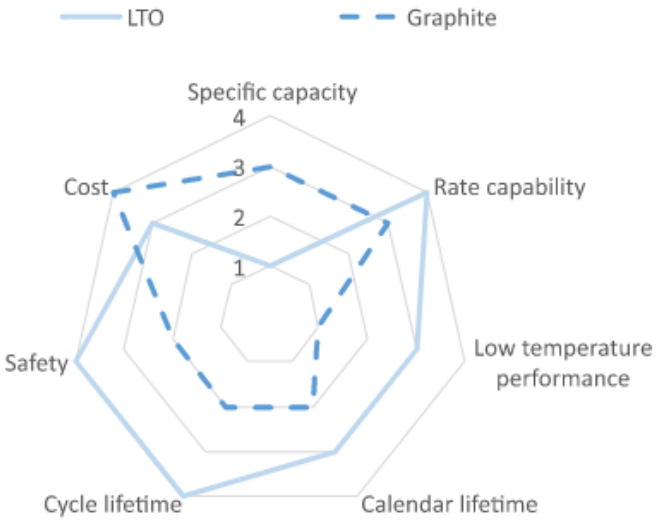

Figure 2.4: Comparing LTO and graphite as anode material in Li-ion cells [22]

The other cell components, in addition to the anode and cathode materials, also affect the cell properties (electrolyte, separator, current collector, housing). The range of properties for a Li-cell with graphite and LTO as an anode can be seen in the Table 2.1.

It can be observed from Table 2.1 and Figure 2.4 that having LTO as the anode can lead to an excellent lifetime even when cycled at a DoD of 100% [23]. This can be explained due to LTO's "zero-strain" property. Since lithium insertion and extraction occur in a highly reversible reaction, this process doesn't significantly change the volume. Therefore, during cycling, the material experiences very little mechanical stress, extending its cycle life. In contrast to cells with graphite anodes, where the potential charge current rate is much lower than the discharge current, LTO anodes enable charge current rates that are as high as the discharge current rates [16]. The electrical, thermal, and aging characteristics of the battery cell are altered when LTO replaces graphite. The energy density of a battery cell is decreased as a result of the spinel-structured LTO's low theoretical specific capacity and high working potential of 1.55V during lithiation and delithiation (resulting in a lower full-cell voltage). However, because of this high potential and thermal properties of LTO anode, the safety is improved [24].

Parameters		Li-ion cells with graphite anodes	Li-ion cells with LTO anode
Nominal cell voltage	V	3.2 – 3.7	1.9 – 2.5
Gravimetric energy density	Wh/kg	120 – 260	45 – 100
Volumetric energy density	Wh/l	300 – 700	80 – 250
Cycle lifetime		500 – 4000	15,000 – 60,000
Temperature range (charge / discharge)	°C	0 – 45 / -20 – 60	-30 – 60 / -30 – 60

Table 2.1: Comparison between LTO vs Graphite as anode for Lithium cells [16]

LTO batteries showcase noteworthy high rate capabilities, resulting in elevated C-rates and consequently, amplified charge and discharge currents. Conversely, graphite-based batteries offer heightened

energy densities, leading to reduced bus weight, and are significantly cheaper than LTO-anode-based batteries. It is therefore necessary, to rigorously subject all three distinct battery chemistries to the exacting demands of IMC bus operations, and factor in cost considerations and the bus's comprehensive lifespan to evaluate the suitability of the three types of battery chemistries.

2.5. Battery aging and modeling

2.5.1. Battery aging mechanisms

According to [25], the most common modes of aging in lithium-ion batteries can be attributed to three main factors:

- The first is the loss of lithium inventory (LLI), which represents the depletion of active lithium ions that are no longer available for cycling.
- The second is loss of active material (LAM), which is the loss of available anode or cathode material as a result of structural degradation.
- The third factor, contact loss, is brought on by the deterioration of electrical parts, such as corrosion of the current collector and decomposition of the binder.

These three modes of aging are significant contributors to the degradation and overall lifespan of lithium-ion batteries.

As reported by Mekonnen et al. [26], graphitic carbon materials are the most commonly used anode materials in batteries. However, in recent years, there has been a growing interest in using LTO as an anode material in batteries [22]. The properties of the graphite electrode are significantly affected by the Solid Electrolyte Interface (SEI), which is the primary factor that contributes to the aging of the graphite electrode [27]. The electrolyte's electrochemical stability window does not encompass the voltages at which negative electrodes based on graphite operate. Therefore, a protective layer is formed due to electrolyte decomposition, known as the SEI [28]. Understanding the mechanisms of SEI formation and its impact on the performance and aging of graphite-based electrodes is crucial for the development of high-performance and long-lasting batteries. As noted by Birkl et al. [29], metallic lithium plating can occur under specific conditions such as low SOC, low temperature, and high C-rates. Vermeer et al. [25] highlighted that his phenomenon results in the deposition of lithium on the anode, which reduces the active surface area and ultimately leads to LLI. The formation of lithium deposits can also cause internal short circuits, which can result in safety hazards and further degradation of the battery.

Similar to the SEI formed at the anode, a surface film known as the Cathode Electrolyte Interphase (CEI) is formed on the surface of the cathode [30]. The CEI is formed due to electrolyte oxidation and salt deposition on the cathode. During the charge and discharge process, both the anode and cathode undergo mechanical stresses that result in structural and volumetric changes. Furthermore, since transition metals are commonly used in battery anodes and cathodes, they can undergo chemical reactions with the electrolyte, leading to their dissolution and deposition on the anode surface [30]. This can result in a reduction of the active surface area of the anode and ultimately lead to the degradation of the battery.

2.5.2. Aging causes

- **Temperature**: Cell temperature impacts the degradation of lithium-ion cells, with high temperatures accelerating the growth of the SEI layer and the chemical decomposition of cell components. Conversely, low temperatures pose risks during cell charging, including lithium plating. Manufacturers typically guarantee service life at around 20 or 25°C, applying to a narrow temperature range [31].
- **Depth of Discharge**: Cycles with DoD induce structural changes in lithium-ion cells, leading to reduced storage capacity. The electrode undergoes volume changes during each charge-discharge cycle due to lithium-ion storage, affecting the grid structure [32].. With increasing cycle count, fewer ions can be stored, resulting in decreased usable cell capacity. Notably, cycles with lower DoD have a relatively minor impact on aging compared to full cycles. Therefore, it's advisable to keep discharge cycles brief. This can be achieved by maximizing opportunities for system recharging or by over-sizing the system to minimize the DoD during cycles.

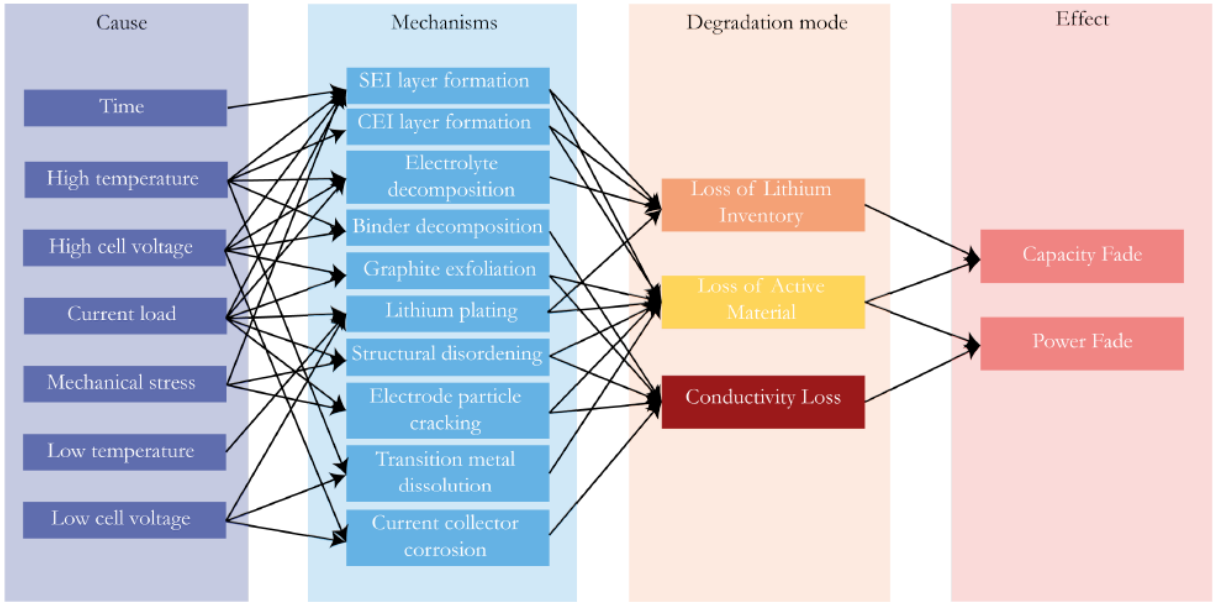

Figure 2.5: Aging processes and their impact on lithium-ion batteries [25]

- **State of Charge**: Calendar aging of batteries is influenced by SOC during storage, and this effect extends to cycle aging. In [33] found that at a 30% average SOC level, cells experience a mere 2.4% capacity loss after 600 cycles. In contrast, the capacity loss is 8.4% at 50% SOC and 9.6% at 70% SOC. This data underscores that lower average SOC levels contribute to reduced aging.
- **C-rate**: Cell stress escalates as the C-rate increases, leading to intensified degradation. This occurs because a higher current in the cell results in a more significant temperature elevation. Hence, a lower C-rate is preferable to mitigate these effects.

2.5.3. Battery modeling

Battery modeling can be categorized into three types:

- Physics-based models (PBMs): Effective modeling of battery systems requires accurate representation of the underlying material properties and reaction mechanisms taking place inside the battery. Electrochemical or physics-based models have been found to be the most effective in achieving this, as they provide a detailed understanding of the system's behavior. However, these models are complex, and their implementation in power systems is challenging due to the presence of nonlinear differential equations and numerous unknown variables [19].
- Electrical circuit models: To overcome challenges of physics-based models, electrical circuit models (ECMs) have been developed that employ electrical components, such as capacitors, resistors, and voltage sources, to represent the battery's current-voltage (I-V) characteristics. Compared to electrochemical models, ECMs have simpler structures and fewer unknown variables, making them more suitable for battery-powered system control models [34]. Various ECMs have been developed for different types of batteries, as demonstrated in studies by Hu et al. [35] and Low et al. [36]. However, there are few models available for lithium titanate oxide (LTO) batteries.
- Empirical and semi-empirical models (EMs) provide an alternative approach to modeling battery systems. Instead of relying on electrochemical or physics-based models, EMs use analytical formulas obtained by fitting the relationship between various stress factors and the available data through curve-fitting techniques. EMs are widely used in various battery-related studies, such as battery management systems, optimization models, and system-level design issues due to their ease of use and versatility [25].

Out of the three models presented above, EMs require minimal input data and can be developed quickly through simple mathematical relationships. EMs also provide a more practical approach to modeling,

Model	Complexity	Accuracy	Amount of data	Applications
PBM	high	high	low	Battery design
ECM	medium	medium	high	SoH estimation
MLM	medium-high	medium	high	SoH estimation
EM	low	low-medium	high	System design and Optimization

Table 2.2: Different types of battery modeling techniques [25]

making them easier to integrate into system-level models. They are useful for studying the effect of different stress factors on battery performance, such as temperature, cycling rates, and state of charge.

An overview of different empirical and semi-empirical models of LFP/C, NMC/C, and LTO batteries available in the literature is presented in Table 2.3. The studies under consideration exhibited variations in their incorporation of stress factors for the purpose of modeling battery aging phenomena. These models investigate both calendar and cyclic aging and merge the two to formulate a comprehensive empirical model. When addressing calendar aging, the stress factors involved are temperature and SOC, whereas cyclic aging is characterized by the integration of different stress factors, as depicted in Table 2.3.

Empirical models are constructed based on experimental results, which are then fitted to mathematical equations to establish a model. Therefore, it is important to carefully consider the range within which the experiments were conducted and to fit the mathematical curves. Calendar aging is dependent upon the battery cell's SOC and temperature. Cells are subjected to storage under specific SOC and temperature. Periodic assessments of their remaining capacity are then conducted. Cycle aging is dependent upon factors including the DoD, average SOC, as well as the charging and discharging C-rates. It is quantified by evaluating cell (Ah) throughput. Cycle aging is evaluated by subjecting the battery to repetitive charge-discharge cycles at specific DoD and C-rate settings. Subsequent measurements of the remaining battery capacity after a defined number of cycles allow for the determination of the rate of aging. The development of empirical models relies on utilizing experimental data encompassing varying stress factor ranges.

The present thesis will use these pre-existing models from the literature to investigate the aging effects within the context of IMC operational conditions. In Table 2.3, the temperature range, DoD range, and C-rate range denote the spans over which the experimental investigations were carried out. On the other hand, the stress factors indicate whether these specific stress factors have been integrated into the aging model or not.

Cell Chemistry	Temp	DoD	Avg. SOC	C-rate	Temp range (°C)	DoD range (%)	C-rates	Source
NMC/C	✓	✓	✗	✗	35 - 50	5 - 100	1C	[37]
NMC/C	✓	✓	✗	✓	10 - 46	50	0.5C - 6.5C	[38]
NMC/C	✓	✓	✗	✓	25 - 45	100	1C	[39]
NMC/C	✓	✓	✗	✗	20	10 - 75	1C	[40]
NMC/C	✓	✗	✗	✓	10 - 45	55 -75	C/3 - 5C	[41]
NMC/C	✓	✓	✗	✗	-10 - 50	10 - 100	C/3 - 2C	[42]
NMC/C	✓	✓	✗	✓	10 - 40	20 - 90	0.5C - 3C	[43]
NMC-LMO	✓	✗	✗	✗	30 - 60	10 - 70	4C	[44]
NMC/C	✓	✓	✗	✗	25 - 45	20 - 100	2C	[45]
NMC/C	✓	✓	✓	✓	-20 - 50	0 - 100	1C - 10C	[31]
NMC/C	✓	✗	✗	✓	10 - 46	50	0.5C - 6.5C	[46]
LFP/C	✓	✓	✗	✗	35 - 50	10 - 80	4C	[47]
LFP/C	✓	✗	✗	✓	0 - 55	100	0.25C - 1C	[48]
LFP/C	✓	✓	✗	✓	30 - 60	10 - 90	0.5C - 10C	[49]
LFP/C	✓	✓	✗	✓	-18 - 40	20 - 100	1C - 15C	[50]
LFP/C	✓	✗	✗	✓	25	100	0.5C - 5C	[51]
LFP/C	✓	✗	✗	✓	36 - 45	-	2.8C - 6C	[52]
LFP/C	✓	✓	✗	✗	30	5 - 100	1C - 3.5C	[53]
LFP/C	✓	✓	✓	✓	-20 - 50	0 - 100	1C - 10C	[31]
LFP/C	✓	✓	✗	✓	25 - 40	-	C/10 - 1C	[54]
NMC/LTO	✓	✓	✗	✗	42.5 - 50	10 - 50	1C - 3C	[55]
NMC/LTO	✗	✓	✓	✓	-	0 - 100	1C - 20C	[31]
NMC/LTO	✓	✓	✗	✗	42.5	10 - 50	2C	[56]

Table 2.3: Stress factors for different cell chemistries (bold - battery models used in this study).

2.6. Financial aspects of IMC

Establishing an infrastructure to support IMC buses is crucial. Overhead contact lines are frequently employed to enable the charging of vehicles on-the-go.

The construction of a traction network constitutes the most expensive aspect of a dynamic charging system, requiring significant financial investment [6]. Sections of the network with contact lines must be long enough to supply the traction batteries with energy that is at least equal to the energy required to complete the catenary-free segment. The minimum amount of traction network coverage necessary for vehicles currently in use ranges from 40% to 50% [57]. By considering the stopping and moving times of a typical IMC bus and analyzing two charging systems for the IMC bus battery charging (regular and adaptive), [58] presents a more precise method for measuring the charging corridor.

As the IMC concept is relatively new, there is a considerable risk associated with its implementation. According to [57], these risks include:

- the risk associated with building up a new catenary system for the buses, with contact lines long enough to provide the batteries with energy at least equal to the energy required to complete the rest of the trip.
- The majority of the cost of an IMC bus (about 50% of the whole vehicle cost) is attributable to the battery installed, which represents the risk connected with the costs of purchasing new vehicles.
- the risk associated with the cost of replacing the battery, since each battery pack operates at a specific SOC level and is subjected to a specific number of life cycles, it is necessary to change the battery pack after a few years of service.

Bartomiejczyk [6] conducted a comparative economic analysis of stationary and dynamic charging for electric buses. The study concluded that dynamic charging has more fixed costs and less variable costs than stationary charging for electric buses. The author employed a discounted life cycle cost analysis to compare the financial viability of stationary-charged and dynamic-charged electric buses. The analysis aimed to identify the extreme life cost values for different input parameters, including vehicle cost, battery replacement cost, and traffic impact on the charging process. The study used the Monte Carlo Statistics modeling method to analyze the different input data parameter settings.

Despite the perceived high cost of constructing traction networks for dynamic charging systems, it is worth noting that such expenses are considerably lower than those required for tram line infrastructure [59]. Additionally, in cases where the tram network is already fully utilized, it may be possible to reuse certain components of the existing infrastructure for building the catenary system of the dynamic charging system.

The acquisition and replacement costs of batteries are a significant source of financial risk, given the rapidly evolving market for electric vehicles and the unpredictable nature of battery life. Therefore, to comprehensively determine the financial implications of implementing an IMC bus, it is essential to thoroughly examine the associated battery costs.

2.7. Research gaps

While several studies have explored IMC bus technologies and their suitability for public transportation [6, 59, 10, 21], notable research gaps persist in this domain. These gaps necessitate further investigation to advance our understanding of intercity IMC buses.

A significant research gap exists regarding long-distance battery-mode travel for IMC buses. To date, no implementation of this nature has been observed. This presents a compelling area for exploration. Specifically, it is crucial to determine the most cost-effective battery chemistries for inter-city travel where a trip may require more than 25 km of battery-mode operation subjected to highly cyclic load demands.

Existing literature used a method for calculating the power requirement using the average energy approach [15]. However, this approach results in a constant power profile, which is insufficient for studying battery aging. Battery aging is significantly influenced by operational cycles, including power fluctuations due to acceleration, deceleration, auxiliary power usage, and regenerative braking. To address this limitation, the development of a dynamic bus model capable of capturing these dynamic power fluctuations is necessary.

An unexplored area pertains to the incorporation of battery aging effects into battery size selection for IMC buses. While some research has used generalized DoD vs. cycles graphs for intra-city buses, this approach is not thorough [60]. IMC scenarios vary in terms of charging powers, leading to different battery aging effects. Research is needed to bridge this gap by integrating the scenario-specific aging of batteries into an optimization framework.

Therefore, the primary objective of this thesis is to conduct a comprehensive analysis of intercity IMC battery technologies, with a focus on their aging characteristics, and cost considerations for intercity operations. Through a series of research questions, this study aims to deepen the understanding of various aspects of IMC battery technologies for intercity travel. Ultimately, the research will provide valuable insights into selecting the most suitable IMC battery technology and size, particularly in the context of highly cyclical load demands.

3

Development of Battery Load Profiles

This chapter is focused on the development of battery load profiles, specifically designed for different charging scenarios of the IMC bus system. A bus model is first constructed, enabling the generation of power traction for route extending beyond the catenary network. To capture the dynamic fluctuations in power and energy across the entire year, auxiliary power is integrated. This critical addition facilitates the holistic calculation of total power requirements, taking into account the inherent variability in bus operations and the temporal fluctuations throughout the year. Different charging scenarios are then created and examined to get profound insights into the charging strategies for IMC bus operations.

3.1. Available data

In order to construct the bus model, it was imperative to obtain the driving profile data for routes outside the catenary system. However, the available dataset from Arnhem bus operations solely encompassed the velocity profile within the catenary network. Hence, it became necessary to develop a suitable velocity profile for the bus while traversing segments outside the catenary infrastructure.

As depicted in Figure 3.1, the total route from Arnhem Centraal to Wageningen Bus Station was considered for the model development. This route encompasses portions where the bus operates beyond the catenary coverage, thus requiring a velocity profile to be generated for this specific section.

Figure 3.1: Line 352 from Arnhem Centraal to Wageningen Bus Station. Bus operates in trolley mode from Arnhem Centraal to Oosterbeek after which it switches to battery mode for the rest of the trip. (*Google Maps*)

The trolley mode of operation extends from Arnhem Centraal to Oosterbeek, Gementeehuis station, after which the bus transitions into battery mode, operating from Gementeehuis station to Wageningen station. The corresponding distances associated with these specific routes are outlined in Table 3.1. It is worth noting that the catenary infrastructure provides coverage for approximately 25% of the total route distance. Consequently, the available velocity and power data pertains exclusively to the segments operating under the catenary.

For the significant portion of the route beyond the catenary coverage, the absence of velocity and power data poses a critical data gap. This leaves a considerable portion of the bus's journey without specific information on velocity profiles and power traction requirements. As a result, addressing this data limitation becomes imperative to comprehensively understand and accurately model the complete energy dynamics of the bus system.

Route	Mode	Distance (km)
Arnhem centraal to Oosterbeek, Gemeentehuis	Trolley	4.3
Oosterbeek, Gemeentehuis to Wageningen bus station	Battery	13
Arnhem centraal to Wageningen bus station		17.3

Table 3.1: Line 352 route trolley-mode and battery-mode distances

The generation of the velocity profile outside the catenary was done by taking into account factors such as acceleration and top speed in accordance with the available dataset inside catenary Figure 3.2, and potential stops. The objective was to create a trapezoidal velocity profile, based on acceleration and top speed data from the dataset under the catenary, thus ensuring that the model captures the intricacies of the non-catenary segments. The velocity and acceleration profile of the bus outside the catenary is presented in Figure 3.3.

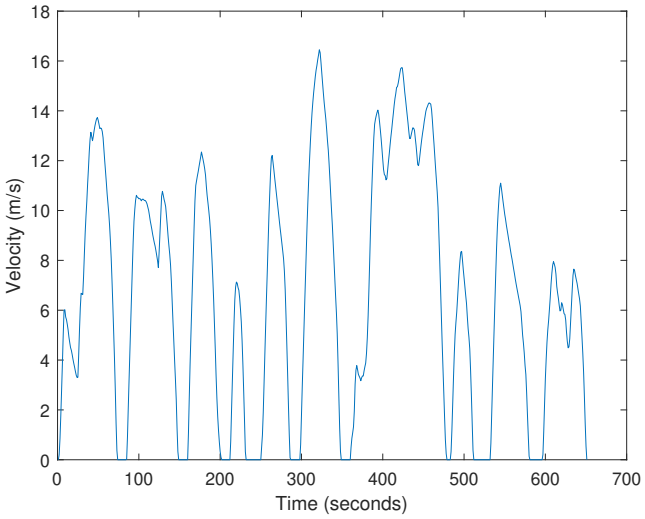

Figure 3.2: Velocity profile under catenary from the Arhhem trolleybus dataset

By synthesizing the velocity profile for the bus along the entire route, the bus model became capable of effectively simulating the power traction required during journeys that extend beyond the confines of the catenary network. This foundational step was necessary for comprehensively evaluating the energy demands of the IMC bus system under investigation.

3.2. Bus model

The generated velocity profile, covering the entire bus route, was the input for the bus model. This bus model takes into account the different forces influencing the vehicle's dynamics. These forces, when combined with the velocity data, yield the essential power requirements for traction.

The formulation of the bus model is based on parameters from the HAN bus model [61]. The specific model parameters used in this study can be found in Table 3.2. However, it is to be acknowledged that certain parameters, namely η (drivetrain efficiency) and η_r (regenerative braking efficiency), had to be assumed due to their absence in explicit documentation. Due to the predominantly flat terrain in the Netherlands, gravitational forces are not taken into account when calculating the total tractive forces. While

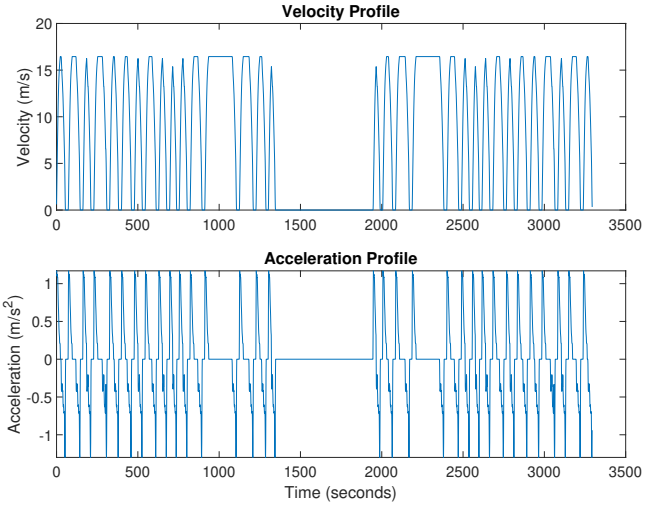

Figure 3.3: Generated velocity and acceleration profile outside the catenary

Parameter	Symbol	Value
Mass	m	18890 kg
Frontal Area	A	8.925 m^2
Coefficient of Drag	C_d	0.8
Rolling coefficient	C_r	0.01
Density of air	ρ	1.225 kg/m^3
Acceleration due to gravity	g	9.81 m/s^2
Drivetrain efficiency	η	0.85
Regenerative braking	η_r	0.7

Table 3.2: Bus parameters taken into consideration for the bus model

this exclusion introduces a level of approximation, the model is still suited for the assessment of various charging scenarios, explained more in detail later in the section.

While the HAN bus model provided a comprehensive representation, this study opted for a simplified version. By focusing on the distinct forces exerted on the bus and their impact on velocity, the simplified model efficiently calculated the power required for traction.

The drag force is given by:

$$F_{\text{drag}} = 0.5 \cdot \rho \cdot C_d \cdot V^2 \cdot A \tag{3.1}$$

The rolling resistance force is given by:

$$F_{\text{roll}} = C_r \cdot g \cdot M \tag{3.2}$$

Force due to acceleration is given by:

$$F_{\text{acc}} = M \cdot a \tag{3.3}$$

$$F_{\text{total}} = F_{\text{drag}} + F_{\text{roll}} + F_{\text{acc}} \tag{3.4}$$

All the above forces together constitute total forces acting on the body. The total tractive power is given by

$$P_{\text{traction}} = \frac{(F_{\text{drag}} + F_{\text{roll}} + F_{\text{acc}}) \cdot V}{\eta} \tag{3.5}$$

Regenerative braking, a notable feature of the deceleration phase, plays a crucial role in recuperating power that can be stored for later use. To account for this energy recovery process, a widely accepted regenerative braking efficiency of 0.7 was adopted. The overall effect of regenerative braking, combined with the influence of other forces acting on the vehicle, is summarized in Table 3.3.

Phase	F_{acc}	F_{roll}	F_{drag}	η_r
Acceleration	yes	yes	yes	NA
Constant Velocity	no	yes	yes	NA
Deceleration	yes	yes	yes	yes

Table 3.3: Forces at different phases of the bus operation

Equation Equation 3.5 provides a representation of the total traction power exerted on the vehicle by taking into account the drivetrain efficiency. However, it is important to acknowledge that traction power is just one component of the entire power consumption picture. The exploration of the total power consumption, encompassing both traction and auxiliary power, is elaborated in Section 3.2.2.

3.2.1. Validation

Before proceeding with the application of the bus model for the computation of traction power outside the catenary, it was important to ensure its accuracy and reliability. To achieve this, a verification process was undertaken, which involved the creation of velocity and power profiles within the catenary region using a similar approach.

The decision to generate velocity and power profiles within the catenary region was prompted by the availability of reliable data in this particular area. By leveraging the bus model, these profiles were constructed, and their representation is illustrated in Figure 3.4.

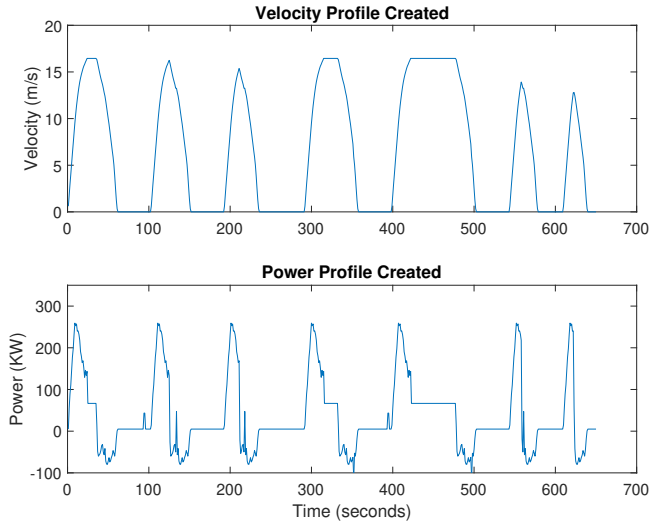

Figure 3.4: Velocity profile and power profile created under catenary

A comparison was conducted between the energy consumption derived from the available data within the catenary network and the corresponding energy values obtained from the profiles created using the bus model. The results of this comparison are clearly presented in Figure 3.5.

The outcome of this analysis was the similarity in the energy consumption patterns across both methods. The energy values derived from the available data and the model-generated profiles exhibited a good

degree of congruence, validating the bus model's accuracy and its ability to capture the energy dynamics within the catenary region.

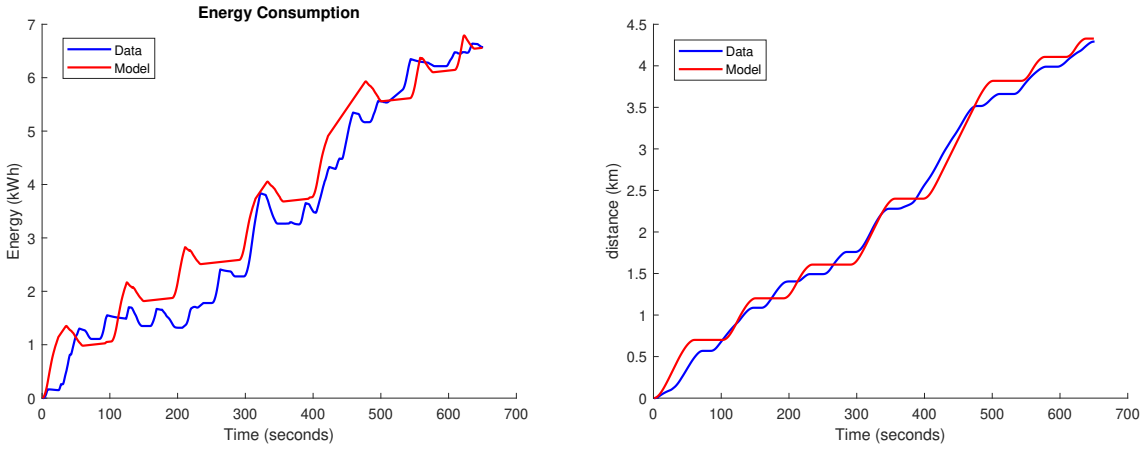

(a) Energy consumption **(b)** Distance travelled

Figure 3.5: Comparison of the energy consumption and total distance calculated from the Arnhem dataset and the created bus model

3.2.2. Year-long profile

Utilizing the bus model, the total traction power for the entire trip from Arnhem Centraal to Wageningen was obtained, as depicted in Figure 3.6. However, it is important to acknowledge that total power consumption consists of two main components: power traction and auxiliary power. Unlike power traction, auxiliary power exhibits high variability, not only on a day-to-day basis but also throughout each day.

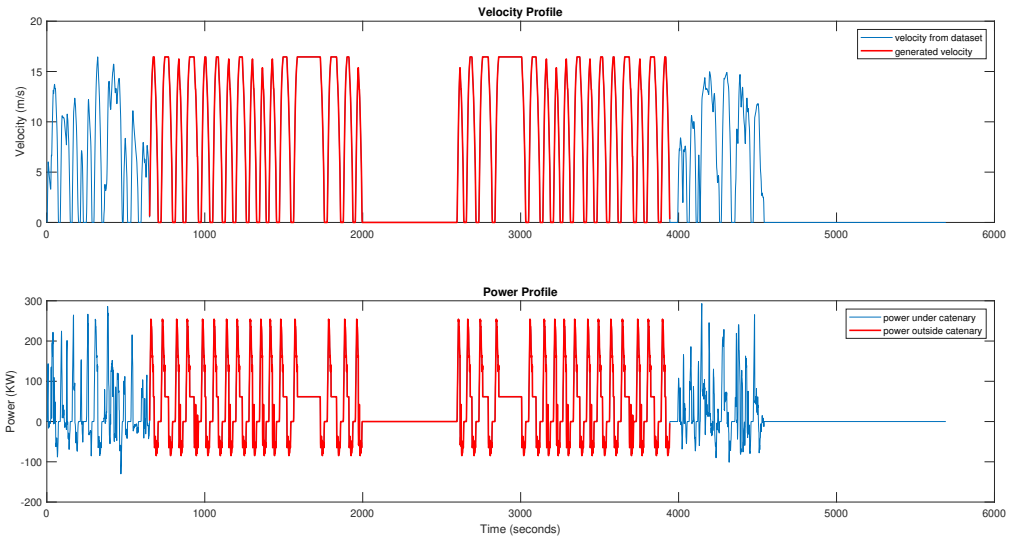

Figure 3.6: Velocity profile and power traction for one trip (blue - velocity and power profiles under the catenary based on Arnhem trolleybus dataset, red - generated velocity and power profile outside the catenary using the bus model)

To comprehensively understand the complete power consumption pattern of the IMC bus system, it is imperative to consider the auxiliary power requirements. This additional factor is essential in obtaining a holistic view of the bus's energy demands over an extended duration.

To incorporate auxiliary power data for the calculation of total energy consumption, overcoming the lack

of available data for buses running in line 352 became essential. To address this data gap, a comprehensive data-gathering effort was undertaken for all trolleybuses running in Arnhem, for which auxiliary power data was available. Notably, since all these buses operate in the same geographical location, and experience similar ambient temperatures, Since the auxiliary power is highly influenced by the ambient conditions, because of the similarities in the ambient temperatures, one can argue the similarity in auxiliary power requirements of buses running in the area.

In order to analyze the auxiliary power patterns, the data for all buses were plotted in the form of average auxiliary power per day, as illustrated in Figure 3.7a. A clear similarity in the daily patterns of auxiliary power among different buses emerged. The minor deviations in auxiliary power, represented by spikes on days close to each other, were primarily attributed to variations in bus schedules.

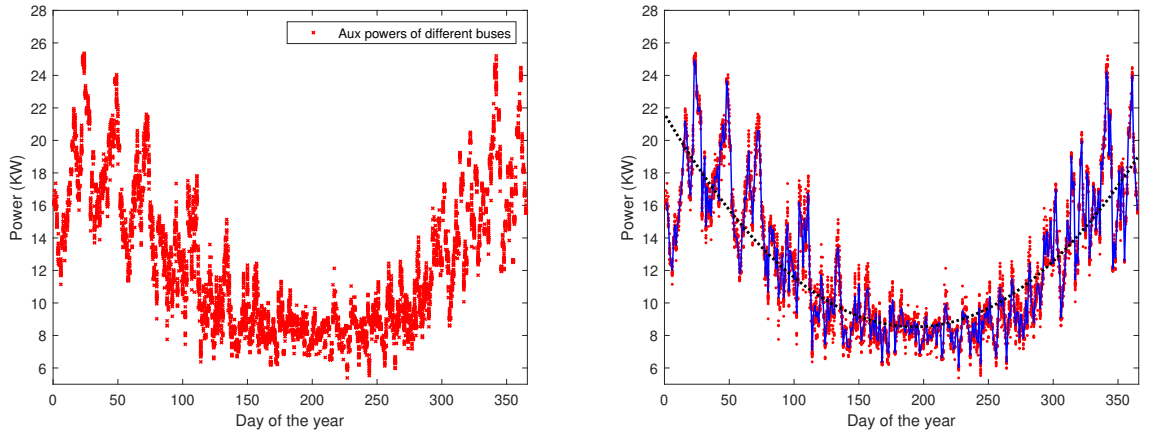

(a) Average AUX power for all buses in Arnhem

(b) Trendline based on averages of AUX power for all buses

Figure 3.7: Average AUX power variation throughout the year

To streamline the analysis, the average of the average auxiliary power of all buses was calculated, and a trendline was developed based on this average data using a polynomial equation, as shown in Equation 3.6.

$$\text{Auxiliary Power (W)} = 0.35\text{W} \cdot d^2 - 135.91\text{W} \cdot d + 21642.69\text{W} \tag{3.6}$$

where d is the day of the year.

Instead of considering the average auxiliary power variation throughout the year, an alternative approach was adopted. After calculating the average of all buses' auxiliary power, a specific bus was selected for which auxiliary power data was available, and it was observed that this bus ran throughout the day. The auxiliary power data from this selected bus was then added to the power traction to calculate the total power consumption of the bus.

As seen in Figure 3.8, there is a similarity between the actual auxiliary power used by this particular bus in Arnhem and the average auxiliary power of all buses. This similarity validates the usage of the average auxiliary power to estimate the total power consumption effectively.

By adopting this approach, the total power consumption of the bus, including both traction and auxiliary power, can be effectively assessed. This methodology enables a comprehensive understanding of the energy demands of the IMC bus system over extended periods.

The results of incorporating auxiliary power into the traction power to obtain the total power consumption can be observed in Figure 3.9 and Figure 3.10. This representation showcases the total energy consumption on different days throughout the year, as displayed in Figure 3.9. It is evident that energy consumption exhibits significant variations during the winter season, reaching levels above 900 kWh per day, while during spring, it decreases to as low as 600 kWh per day.

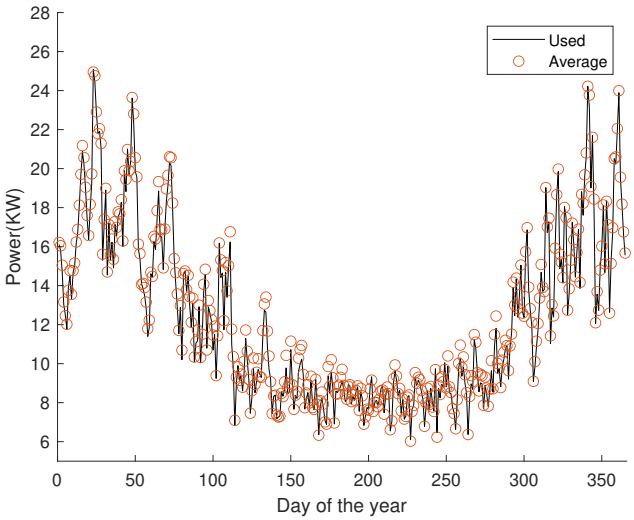

Figure 3.8: Average of auxiliary power used to calculate the total power consumption of the bus of line 352 vs average of auxiliary power all trolleybuses in Arnhem combined

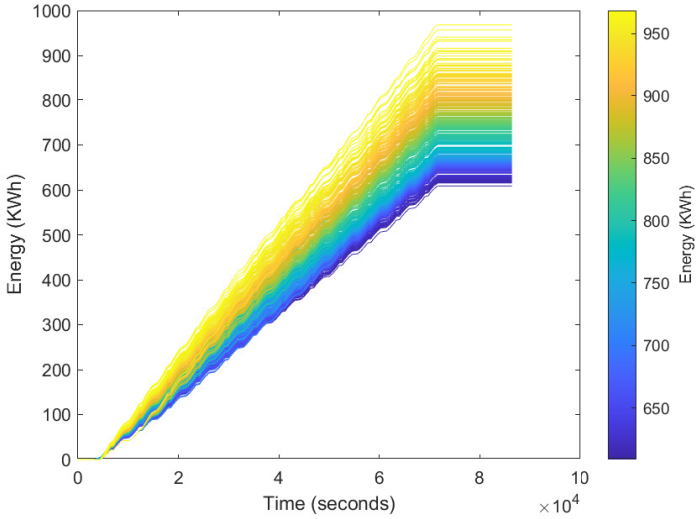

Figure 3.9: Daily energy consumption for bus line 352 over the course of a year

Another perspective to consider the energy consumption is by examining the energy consumption per kilometer, as shown in Figure 3.10. The pattern of energy consumption per kilometer mirrors that of the total energy consumption, as the total distance traveled per day remains consistent. During winter, the energy consumption per kilometer can be as high as 2.3 kWh/km, while during spring, it may decrease to as low as 1.5 kWh/km.

By considering the auxiliary power variations throughout the year, the total power consumption of the intercity IMC bus was successfully developed. This approach accounts for the dynamic nature of energy demands and presents a comprehensive understanding of the bus system's energy consumption extended durations.

3.3. Battery charging and discharging

The total power and energy requirements of the bus have been calculated in the previous section. As seen in Figure 3.1 and Table 3.1, the specific route segment from Arnhem Centraal to Oosterbeek,

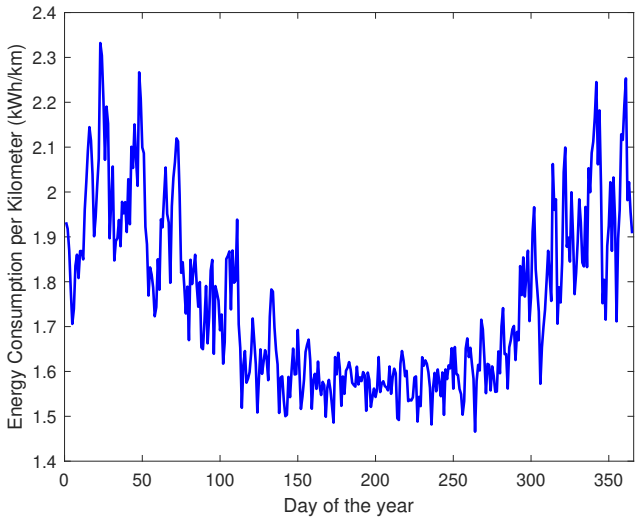

Figure 3.10: Average energy consumption per km for the bus of line 352

Gemeentehuis is under the catenary infrastructure. During this particular section of the journey, the bus's power requirements are fulfilled by the overhead charging system. Simultaneously, the onboard battery charging process takes place, enabling the accumulation of energy reserves to support subsequent phases when the bus operates outside the catenary network.

3.3.1. Battery charging under catenary

The regular charging approach has been chosen for implementation in this study. The rationale behind this decision lies in its current application in Arnhem and other IMC pilot projects. Additionally, the other methods, particularly adaptive and valley charging, involve multiple subcycles of charging, which may potentially impact the battery's lifetime significantly.

The battery charging profile under the catenary, as depicted in Figure 3.11, adheres to the regular charging approach. During motion, the charging power is maintained at 150 kW, while when the bus is stationary, the charging power is reduced to 60 kW. This deliberate reduction in charging power during standstill serves the purpose of preventing overheating and potential damage to the connection point between the bus and the overhead catenary.

3.3.2. Battery discharge outside catenary

During the journey between Oosterbeek, Gemeentehuis, and Wageningen Bus Station, the bus operates in battery mode, relying on the battery to meet both the total power and energy requirements of the vehicle. In this phase, the battery discharges its stored energy to power the bus.

Additionally, the bus benefits from regenerative braking during this phase. This results in charging the battery with the surplus electrical energy generated during braking, allowing the battery to store the recuperated energy for later use, which results in an extension of the range of the bus. The discharging phase can be seen in Figure 3.12.

3.4. Charging scenarios

In this section, various charging scenarios are developed using the charging and discharging profiles created in earlier sections. The objective of these charging scenarios is to investigate and compare their respective benefits for IMC buses. Each charging scenario is distinguished by the IMC bus charging power applied inside the catenary, which can potentially have different effects on the health of the bus's battery.

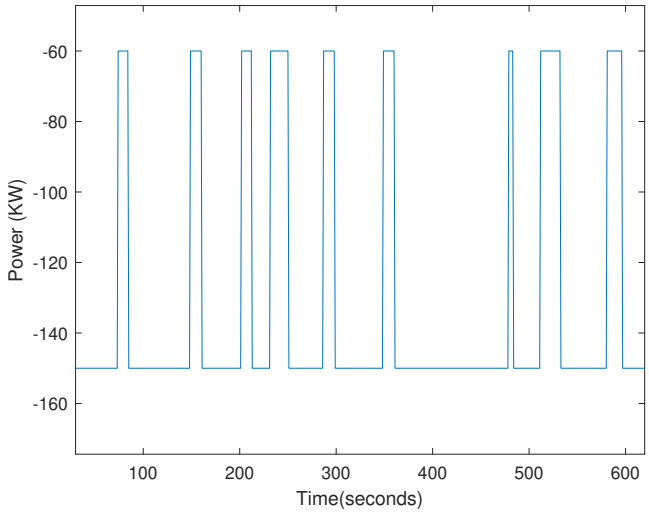

Figure 3.11: Battery charging profile under catenary between Arnhem Centraal and Oosterbeek, Gemeentehuis

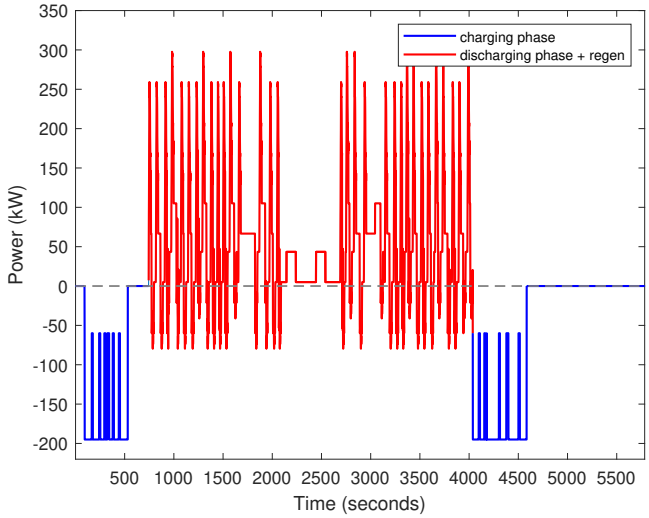

Figure 3.12: Battery load profile for in-motion charging only for bus line 352 for a round trip from Arnhem Centraal to Wageningen bus station

Four distinct charging scenarios have been considered and are explained in this section. The scenarios and their charging power and charging locations can be seen in Table 3.4. These scenarios are designed to capture different charging strategies and their potential impacts on the battery. By studying and analyzing these charging scenarios, valuable insights can be gained into their effect on charging power requirements and battery health, ultimately identifying the most advantageous charging approach for IMC buses.

Scenario	**Charging Powers**		
	under catenary	at Arnhem Centraal	at Wageningen
IMC only (Scenario 1)	195 kW / 60kW	-	-
IMC with stationary charging (Scenario 2)	125 kW / 60kW	60 kW	-
IMC with opportunity charging (Scenario 3)	100kW / 60kW	-	200kW
IMC with overnight charging (Scenario 4)	125 kW / 60 kW	50 kW	-

Table 3.4: Different charging scenarios and charging powers

3.4.1. In-motion charging only

The first charging scenario examined involves exclusive in-motion charging, limiting the battery charging process to occur only when the bus is in motion between Arnhem Centraal and Oosterbeek, Gemeentehuis. During the stationary period at Arnhem Centraal stop, the bus does not undergo any charging to prevent grid congestion at the Centraal bus station, which accommodates multiple other buses.

As the bus charges solely under the catenary during motion between Arnhem Centraal and Oosterbeek, Gemeentehuis, the charging power is of crucial significance. As the battery depletes its energy during the discharge phase, it has only a specific duration (equal to the time spent under the catenary) to recharge sufficiently and meet the energy requirements for subsequent trips.

A battery size of 58 kWh, operating at 100% DoD is found to meet the operational demands of the trip. The SOC graphs of a battery sized to fulfill the maximum energy requirements throughout the year indicate that charging powers of 120 kW, 150 kW, and 180 kW are insufficient to meet the bus's energy demands consistently as seen in Figure 3.13 to Figure 3.15. However, when the charging power is increased to 195 kW, the battery becomes capable of charging adequately to sustain all trips within the specified charging time under the catenary as shown in Figure 3.16. This charging power allows the bus to maintain a reliable operation while utilizing the available charging time and maximizing the bus's range without compromising the battery's ability to meet operational demands. The load profile of the battery can be seen in Figure 3.12.

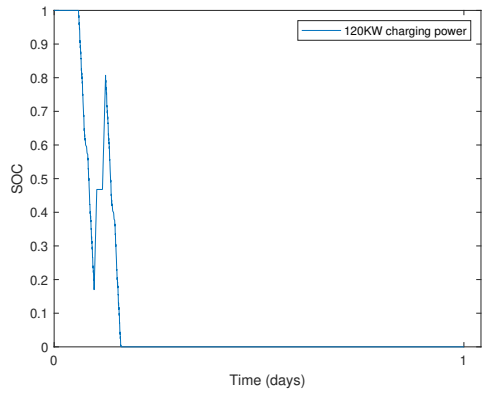

Figure 3.13: SOC profile for 120kW IMC power under catenary for scenario 1: battery insufficiently charged to fulfill daily operational needs

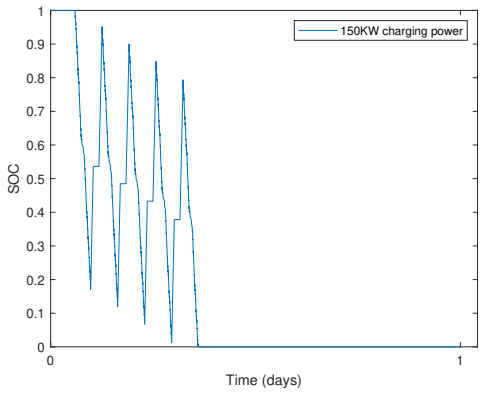

Figure 3.14: SOC profile for 150kW IMC power under catenary for scenario 1: battery insufficiently charged to fulfill daily operational needs

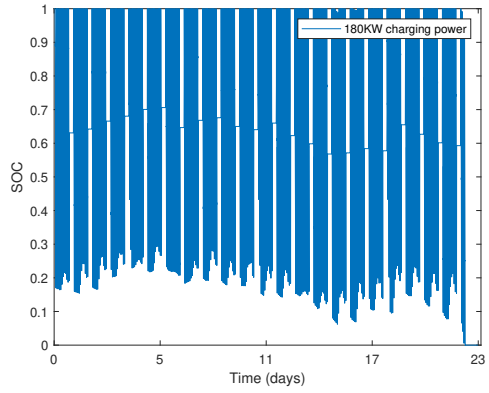

Figure 3.15: SOC profile for 180kW IMC power under catenary for scenario 1: battery insufficiently charged to fulfill daily operational needs

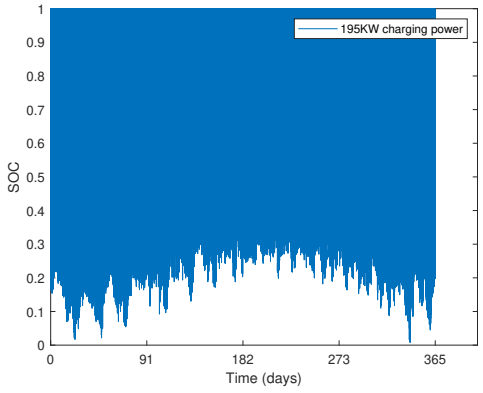

Figure 3.16: SOC profile for 195kW IMC power under catenary for scenario 1: battery sufficiently charged to fulfill daily operational needs

3.4.2. In-motion charging with stationary charging at Arnhem

In order to address the issue of high charging power under the catenary in the previous scenario, a stationary charging system is introduced during the transition between the end and the start of a new trip. This system incorporates an idle time of 1200 seconds, during which the charging power is set at 60 kW, the same power used when the bus is at stops. The stationary charging system can easily be extended to areas where a trolleybus overhead line exists, such as Arnhem Centraal bus station. These stationary charging systems are constrained by the maximum current capacity of the pantograph collector, which is approximately 300 A, selecting a charging power of 60 kW remains well within the system's operational limits [6].

By increasing the charging time at Arnhem Centraal, it becomes possible to reduce the charging power required under the catenary. Figures 3.17 depict the charging power under the catenary, showcasing values of 100 kW and 120 kW. However, both these scenarios lead to the battery being unable to meet the operational demands on day 15 and day 341, respectively. The limited charging time does not allow the battery to charge sufficiently to meet the subsequent discharge demands. Only by setting the charging power under the catenary to 125 kW can the battery adequately meet the operation demands throughout the year, with the maximum depth of discharge reaching 100. The battery load profile for a single trip is displayed in Figure 3.18.

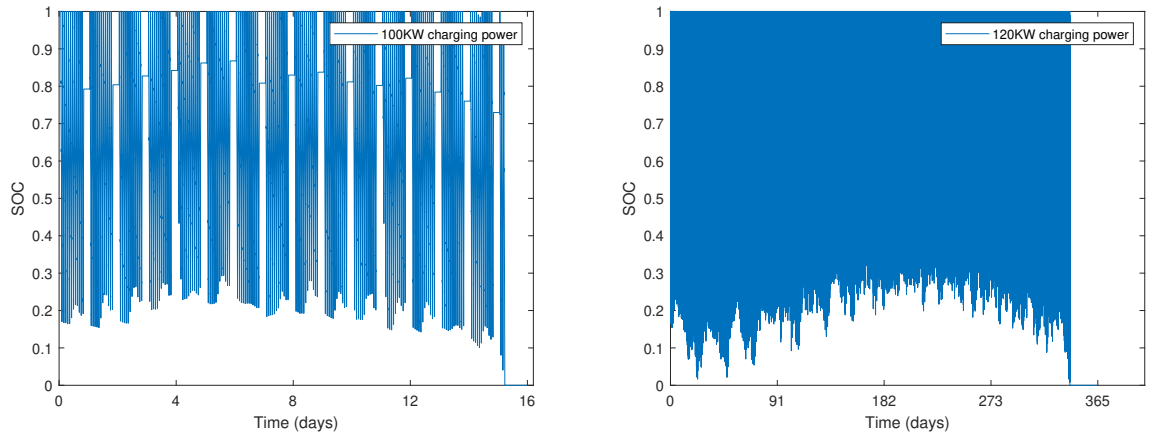

(a) SOC profile for 100kW IMC power under catenary for scenario 2: battery insufficiently charged to fulfill operational needs

(b) SOC profile for 120kW IMC power under catenary for scenario 2: battery insufficiently charged to fulfill operational needs

Figure 3.17: SOC profiles for different IMC powers with 60kW stationary charging at Arnhem

The introduction of the stationary charging system exemplifies an effective approach to balance charging power under the catenary while ensuring sufficient battery charging for uninterrupted operation. This solution holds the potential to improve the IMC bus operation by reducing its dependency on the trolley grid for high-charging power.

3.4.3. In-motion charging with opportunity charging in Wageningen

Due to the given time constraint, a charging power of 200 kW is chosen for the opportunity charging at Wageningen station. This charging power has been determined to be sufficient to recharge the battery adequately during the stop, enabling the bus to cover the distance on battery mode before entering the trolley grid again for the return trip, as demonstrated in Figures 3.19 to 3.22. Opportunity chargers of 100 kW, 120 kW, and 150 kW are unable to meet the seasonal requirement of the trip. This is achieved by using a battery size of 27 kWh operating at 100% DoD, which is capable of meeting the operational demands of this trip.

With the introduction of this opportunity charging at Wageningen station, the charging power required under the catenary is now reduced to just 100 kW. This reduction in catenary charging power is a result

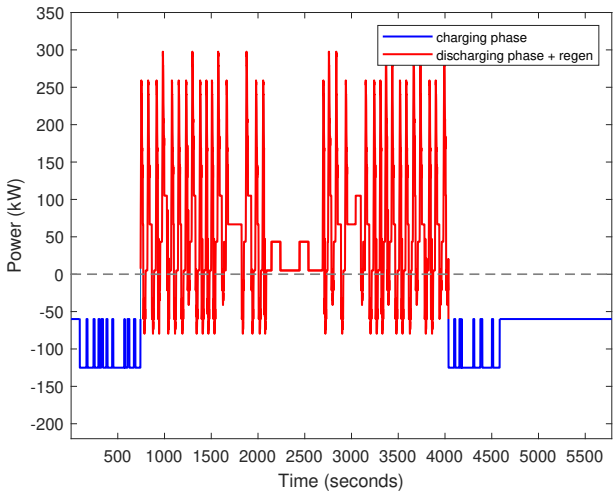

Figure 3.18: Battery load profile for In-motion charging with stationary charging at Arnhem for bus line 352 for a round trip

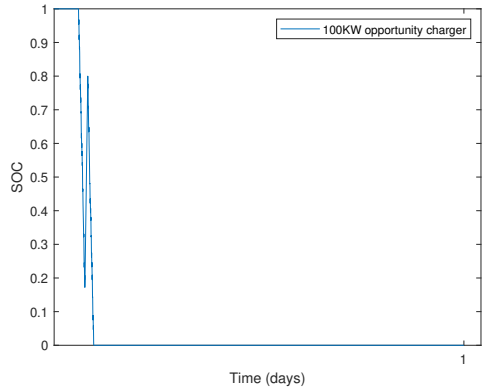

Figure 3.19: SOC profile with 100kW opportunity charger, 100kW IMC power: battery insufficiently charged to fulfill daily operational needs

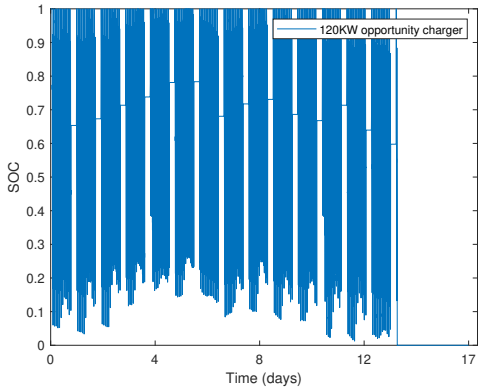

Figure 3.20: SOC profile with 120kW opportunity charger, 100kW IMC power: battery insufficiently charged to fulfill daily operational needs

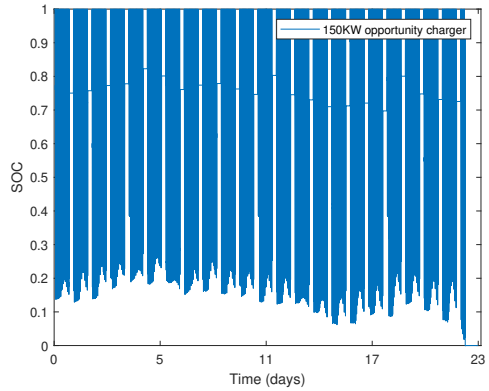

Figure 3.21: SOC profile with 150kW opportunity charger, 100kW IMC power: battery insufficiently charged to fulfill daily operational needs

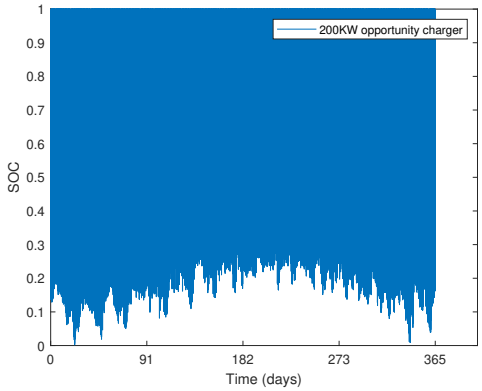

Figure 3.22: SOC profile with 200kW opportunity charger,100kW IMC power: battery sufficiently charged to fulfill daily operational needs

of the opportunity charging at the midway point, which significantly decreases the amount of energy the battery needs to be charged while operating under the catenary.

It is important to note that altering the opportunity charging power and adjusting the catenary charging power for larger battery sizes can be explored. However, increasing the catenary charging power may lead to grid congestion and other practical challenges. Therefore, for this reason, a lower charging power under the catenary of 100 kW has been determined to be sufficient to fully charge the battery, especially when combined with the opportunity charger at Wageningen, for a battery sized to handle a maximum of 100% DoD. The battery load profile for a single trip is displayed in Figure 3.23.

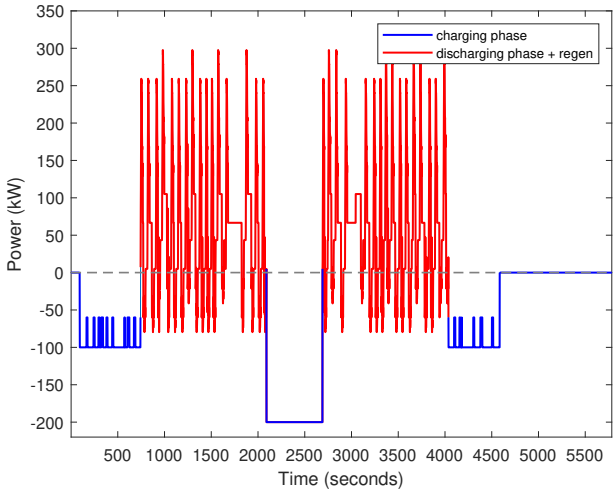

Figure 3.23: Battery load profile for in-motion charging with opportunity charging at Wageningen for bus line 352 for a round trip

Therefore the potential benefits of an opportunity charging station at Wageningen station for the IMC bus system are:

- Reduced battery size: The bus now only needs to cater to half of the round trip between Arnhem Centraal and Wageningen station before recharging. As a result, the required battery size can be reduced (from 58 kWh to 27 kWh, potentially leading to cost savings demanding its effect on battery health.
- Lower charging power under the catenary: As the battery capacity that needs to be charged has halved due to the opportunity to charge at Wageningen station, the charging power required under the Catenary can also be reduced.
- Elimination of stationary charging at Arnhem Centraal: The introduction of opportunity charging at Wageningen station eliminates the need for the stationary charging system at Arnhem Centraal.

3.4.4. In-motion charging with overnight charging at Arnhem

The final charging scenario considered involves overnight charging at the depot (Arnhem) in addition to in-motion charging. Stationary charging at the depot typically utilizes lower charging power, typically ranging between 30 kW to 60 kW. In this study, a charging power of 50 kW was chosen for the overnight charging at the depot. The total idling time at the depot is 5 hours, providing ample time for the battery to charge up to 250 kWh at this charging power.

Implementing overnight charging at the depot offers the advantage of reducing the required charging power under the catenary. However, it also results in a larger battery capacity, which becomes a limiting factor to consider. This situation poses a crucial decision-making challenge: choosing between a higher charging power under the catenary or a larger battery capacity to ensure the bus meets its operational needs throughout the year.

Upon examination, it was observed that with a 100 kW charging power under the catenary, the required battery capacity to meet operational demands is 370 kWh as seen in Figure 3.24. On the other hand, when the charging power under the catenary is increased to 125 kW, the battery capacity needed to meet operational demands is reduced to 250 kWh as shown in Figure 3.25. This significant reduction in required

battery size when compared to the increase in charging power becomes more dominant. Therefore, a charging power of 125 kW under the catenary and 50 kW for overnight charging at the depot has been chosen. The load profile for the last trip of the day and the start of the subsequent day can be seen in Figure 3.26. This load profile showcases the battery's charging and discharging patterns.

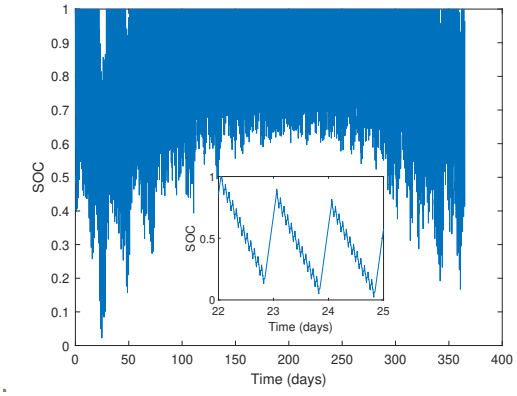

Figure 3.24: SOC profile of a 370 kWh battery with 100kW IMC power, and 50kW overnight charging power

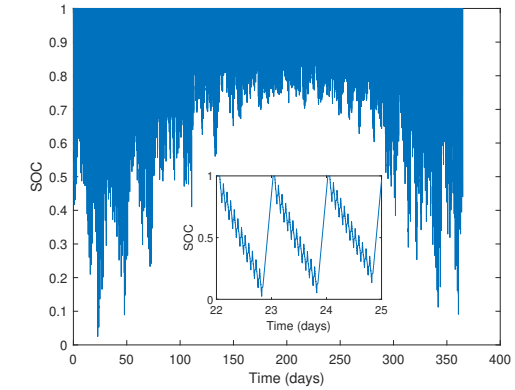

Figure 3.25: SOC profile of a 250 kWh battery with 125kW IMC power, and 50kW overnight charging power

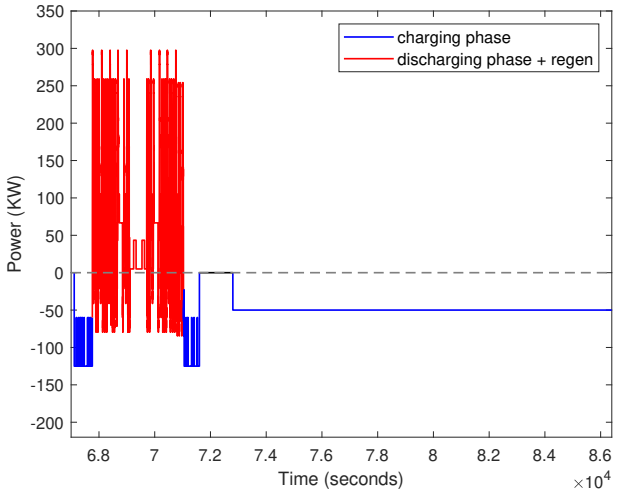

Figure 3.26: Battery load profile for in-motion charging with overnight charging at Arnhem of bus line 352

3.5. Summary

In this chapter, a bus model capable of generating power traction for routes outside the catenary network is created. Auxiliary power is incorporated to consider power and energy variations throughout the year, resulting in the total power requirements. The different charging scenarios are then discussed.

The first charging scenario involves only in-motion charging, where the battery is charged solely during the bus's motion between Arnhem Centraal and Oosterbeek, Gemeentehuis. Charging during stationary periods at Arnhem Centraal is avoided to prevent grid congestion. The required charging power under the catenary becomes crucial for the battery to meet operational demands. Different charging powers are explored, and a charging power of 195 kW is found to be sufficient. To reduce charging power under the catenary, a stationary charging system is introduced at Arnhem Centraal during the transition between trips. The charging power under the catenary is decreased to 125 kW long with a 60kW stationary charging at Arnhem Centraal. This scenario ensures the battery is fully charged for the entire trip. Opportunity charging at Wageningen station is introduced as the next scenario. An opportunity charging system with a charging power of 200 kW is implemented during bus stops at Wageningen station. This allows for a reduction in catenary charging power to 100 kW. A battery capacity of 27 kWh is found sufficient to meet operational demands. The final scenario combines overnight charging at the depot (Arnhem) with in-motion charging. The charging power at the depot is set to 50 kW, IMC charging at 125 kW, and the battery capacity is 250 kWh.

In the subsequent chapters of the thesis, various battery chemistries suitable for onboard storage in the intercity IMC bus system will be explored and compared. The performance of these different battery chemistries will be thoroughly analyzed in terms of battery health. This analysis will involve conducting simulations to gain valuable insights into how each charging scenario affects the aging process of the batteries. By simulating the aging process under various charging scenarios, the thesis aims to identify which battery chemistry, when combined with specific charging approaches, offers the best compromise between battery size and DoD.

The optimization sizing of the batteries will be performed based on a careful trade-off between battery capacity and the extent of DoD allowed during operation. The objective is to determine the most cost-effective and efficient combination of battery size and charging approach to ensure reliable operation and prolong battery life.

4

Battery aging

In this chapter, the focus is on understanding battery aging in the context of different charging scenarios for LFP, NMC, and LTO batteries. Various semi-empirical battery models sourced from the literature are employed. By considering different charging scenarios, the effect of each charging approach on battery aging is studied using these battery models. The aim is to assess how different charging strategies impact the long-term lifespan of LFP, NMC, and LTO batteries. The findings from this chapter will serve as a foundation for making informed decisions regarding the selection of the most suitable battery chemistry and charging scenario for the intercity IMC bus system.

4.1. Aging models

In the literature section, an in-depth analysis of various aging models was conducted, this section will focus on the models presented in [38] and [49]. The models considered utilize different algorithms to calculate battery cycles, calendar aging, and cyclic aging. By analyzing the results of both models for the same battery chemistry, valuable insights can be gained regarding the effectiveness and applicability of these empirical approaches. It is expected that the models will produce different outcomes due to their distinct methodologies.

4.1.1. LFP model 1

An empirical capacity fade model for LFP was developed in [49]. The stress factors taken into account for aging mode are the state of charge and temperature for calendar aging, and the temperature and the current for cycle aging.

$$Q_{\text{cal}} = B_{\text{cal}}(\text{SOC}) \cdot e^{-\frac{E_{\text{cal}}}{RT}} \cdot t^{z_{\text{cal}}} \tag{4.1}$$

where in this expression B_{cal} is a pre-exponential factor depending on SOC, E_{cal} is the activation energy, expressed in J/mol, which evaluates the dependency of calendar aging on temperature T, expressed in K, and z_{cal} is a dimensionless constant linked to SEI growth. The parametric values are given in 4.1.

$$Q_{\text{cyc}} = B_{\text{cyc}}(I) \cdot e^{-\frac{(E_{\text{cyc}} + \alpha|I|)}{RT}} \cdot A_h^{z_{\text{cyc}}} \tag{4.2}$$

where B_{cyc} is a pre-exponential factor, z_{cyc} depends on current, E_{cyc} is an activation energy for cycle aging, α is a coefficient for aging acceleration due to current expressed in A, z_{cyc} is an exponent constant that is around 0.5 for a diffusion-limited process. A_h stands for Ampere-hour (Ah) throughput, which represents the amount of charge sent into the cell. These parameter values can be seen in Table 4.2.

Calendar Aging			
$B_{\text{cal}}(\text{SOC})$	30%	65%	100%
	7.34×10^{-5}	6.75×10^{-5}	2.18×10^{-5}
$Ea_{\text{cal}}(\text{SOC})$	30%	65%	100%
	73369 J/mol	69804 J/mol	56937 J/mol
$z_{\text{cal}}(\text{SOC})$	30%	65%	100%
	0.943	0.900	0.683

Table 4.1: Parameters of calendar aging for LPF model 1 [62]

Cyclic Aging				
$B_{\text{cyc}}(I)$	1A	4A	12A	20A
	3.16×10^{-3}	2.17×10^{-4}	1.29×10^{-4}	1.55×10^{-4}
Ea_{cyc}	31700 J/mol			
z_{cyc}	0.55			
α_{cyc}	370.3			

Table 4.2: Parameters of cyclic aging for LFP model 1 [62]

4.1.2. NMC model 1

An empirical framework was formulated by in [38] to address both calendar and cyclic aging processes. Within the framework of the calendar-life equation, the model incorporates a square root relationship with respect to time, effectively capturing the influence of diffusion-limited capacity loss. Furthermore, an Arrhenius correlation is employed to encapsulate the temperature-dependent effects. In terms of cyclic aging, the model establishes an exponential relationship in relation to the C-rate, complemented by a linear correlation with the parameter A_h. Notably, the modeling was done under the constraint of 50% DoD.

$$Q_{\text{cal}} = A \cdot e^{-\frac{E_{\text{a}}}{RT}} \cdot t^{0.5} \tag{4.3}$$

$$Q_{\text{cyc}} = (a \cdot T^2 + b \cdot T + c) \cdot e^{(d \cdot T + e) \cdot \text{C}_{\text{rate}}} \cdot \text{A}_h + f \cdot t^{0.5} \cdot e^{-\frac{E_a}{RT}} \tag{4.4}$$

The values of the coefficient used are given in Table 4.3.

Coefficient	Value	Unit
a	8.61×10^{-6}	1/Ah-K^2
b	-5.13×10^{-3}	1/Ah-K
c	7.63×10^{-1}	1/Ah
d	-6.7×10^{-3}	1/K-(c_rate)
e	2.35	1/(c_rate)
f	14876	1/$\sqrt{\text{day}}$
Ea	24500	J/mol

Table 4.3: Parameteric coefficients for NMC model 1 [63]

This model, along with the one detailed in Section 4.1.1, was reconstructed in MATLAB based on literature references and further validated for its applicability by [64]. It is noteworthy that the validation process employed a cycle counting technique known as the zero-crossover method. This method involves discerning discharge and charge cycles by observing power profiles intersecting the zero line: positive

power values corresponded to discharge cycles, while negative power values indicated charge cycles. Thus, despite variations in the specific parameters employed for calculating battery aging, both models adhere to a shared cycle counting framework.

4.1.3. Open-Sesame models

The second model utilized in this study is sourced from Open-Sesame, a component of IEA Annex 32. Open-Sesame involves comprehensive simulations, offering a platform to investigate battery behavior and performance. Within Open-Sesame, an array of li-ion chemistries, namely LFP, NMC, and LTO, are incorporated. Each cell within this simulation framework is characterized by a distinct chemical library, containing specific traits and attributes.

Stress factors play a pivotal role in characterizing the impact of influential variables, such as the current, C-rate, and average SOC on the aging process of a battery. These stress factors describe the contributions of both calendrical and cyclical aging phenomena. The cumulative aging effect is subsequently computed by adding the influences of calendar-induced and cyclically-induced degradation.

The foundational step in the aging calculation process is degradation under standardized conditions. These degradation metrics were obtained through rigorous laboratory tests which act as a baseline scenario. This initial degradation assessment serves as a cornerstone for comprehending the aging dynamics of the battery over its operational lifespan.

Open-Sesame employs a comprehensive set of six stress factors influencing the state of health (SoH). Leveraging these stress factors, the current states of the battery cell, including SOC, C-rate, and cell temperatures, are considered in the degradation analysis.

Stress Factor	**LFP**	**NMC**	**LTO**
Calendar (SOC)	Yes	Yes	Yes
Calendar (Temperature)	Yes	Yes	Yes
Cyclic (Temperature)	Yes	Yes	No
Cyclic (Avg SOC)	Yes	Yes	Yes
Cyclic (DoD)	Yes	Yes	Yes
Cyclic (C-rate)	Yes	Yes	Yes

Table 4.4: Stress factors for different cell chemistries in Open-Sesame models for LFP, NMC, LTO battery

The quantification of degradation is intricately tied to the stress factors. When a stress factor surpasses unity (unity being the reference case), degradation is accentuated beyond the reference benchmark, underscoring its heightened effect. Conversely, if the stress factor falls below one, degradation is subdued in comparison to the reference. In instances where the influence of a stress factor on battery aging remains unclear or laboratory data is inconclusive, the stress factor is set to one. This approach ensures that neither exaggerated nor diminished degradation occurs, aligning with the reference condition. These stress factors, functioning as dynamic variables, were methodically devised based on the outcomes of prolonged laboratory measurements. However, certain stress factors faced constraints due to limited data availability, resulting in their initialization at a constant value of one, in line with the aforementioned approach.

Calendrical aging, a crucial aspect of battery degradation analysis, is computed at every discrete time step. This calculation is based on a composite of factors, including the degradation under standard conditions, the dynamic influence of stress factors, and the temporal resolution inherent to the simulation. Conversely, temporal resolution plays a negligible role in the calculation of cyclical aging. Cyclic aging depends on each distinct cycle that is identified within the simulation. The determination of a cycle's progression, relative to a full cycle, hinges upon the DoD experienced during that cycle. The cycle counting algorithm employed is the rain flow counting method. This method facilitates the identification and quantification of subcycles, subsequently enabling the calculation of average charge and discharge rates (C-rates) as well as DoD values based on these subcycles. This approach ensures an accurate assessment of the battery's operational dynamics.

The degradation analysis unfolds in a sequence of steps. Initially, calendrical aging is calculated at every time step, encompassing the full span of the simulation. Subsequently, these calendrical aging values are integrated with the outcomes of cyclical aging calculations.

The combination of these stress factors within the Open-Sesame framework provides a nuanced understanding of battery aging by accounting for multiple influential factors. The models implemented from Open-Sesame will be denoted as ”Model 2” for (LFP) and (NMC) chemistries in the subsequent discussions.

4.2. Simulation results

To examine the behavior of these models under input conditions represented by the battery load profile, a series of simulations were conducted for each scenario outlined in Chapter 3. These simulations are carried out for different battery sizes, factoring in their contribution to the overall weight of the bus. To maintain weight constraints, the upper limit for the battery technology's weight on the bus was set at 3 tons. The end-of-life (EOL) criteria was chosen to be 80% of the initial battery capacity. Accordingly, battery sizes adhering to these weight limitations were subjected to aging simulations.

It is pertinent to observe that augmenting the battery size correspondingly resulted in a reduction of both the DoD and the charge/discharge rate (C-rate) for each individual cell. This phenomenon stems from the redistribution of the total current across a greater number of cells in parallel, stemming from the increase in battery size. The term DoD, as used henceforth, specifically pertains to the DoD on the day when the load attains its peak. Notably, it is plausible for the same battery capacity to exhibit varying DoD levels while completing trips in distinct seasons.

The simulations encompassed a range of SOC profiles spanning the entirety of the year. When graphing the outcomes, it's important to note that the y-axis represents the EOL state of the battery, while the x-axis corresponds to the DoD. However, this DoD value on the x-axis reflects the maximum DoD attained by the battery over the course of its year-long operation. In other words, it signifies the peak DoD experienced by the battery during its various operational scenarios throughout the entire year.

The rationale for displaying the peak DoD on the x-axis, rather than the average DoD, stems from the need to ensure the reliability of the selected battery size across varying operational scenarios. In the context of battery sizing, using the average DoD as the x-axis parameter could potentially result in the selection of a battery size that adequately meets average demand conditions but falls short during instances of peak demand and stress. This scenario could lead to operational challenges. Therefore, even though the aging results are based on the average DoD of the battery, the adoption of peak DoD on the x-axis represents a strategic decision that allows for the selection of a battery that meets seasonal operational demands. The results can be seen in Figures 4.1 to 4.3.

4.2.1. LFP comparison

In Scenario 1 and 3, the behavior exhibited by both Models 1 and 2 for LFP demonstrates a degree of similarity. It is noteworthy, however, that Model 1's slight deviations from this trend can be attributed to its foundation on the preexponential factor, denoted as B_{cyc}, which is dependent on prevailing current levels. This becomes very apparent in scenario 2. Notably, within specified current limits, as outlined in [64], the model adopts a predetermined constant value. The battery in Scenario 2 encounters sustained high currents surpassing a certain threshold for extended periods, consequently leading to elevated degradation levels. This phenomenon underscores a limitation inherent in the original MATLAB model implementation. Moreover, the introduction of additional charging time at Arnhem Centraal contributes significantly to aging in comparison to maintaining a constant high-power charging under the catenary. This effect can again be attributed to the influence of B_{cyc}. Furthermore, an interesting observation emerges when examining very low DoD levels, wherein Model 1 exhibits superior performance compared to Model 2. This phenomenon can be attributed to the behavior of B_{cyc} in Model 1 under these specific conditions. In instances of low DoD, which corresponds to larger battery sizes and consequently lower c-rates for individual cells, the value of B_{cyc} for low current levels is low. This reduction in B_{cyc} values translates to lower aging rates, thereby extending the EOL of the battery.

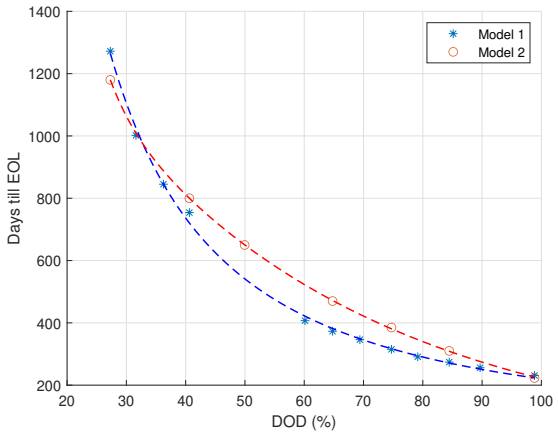

(a) Comparison between LFP Model 1 [62] and Model 2 [31]

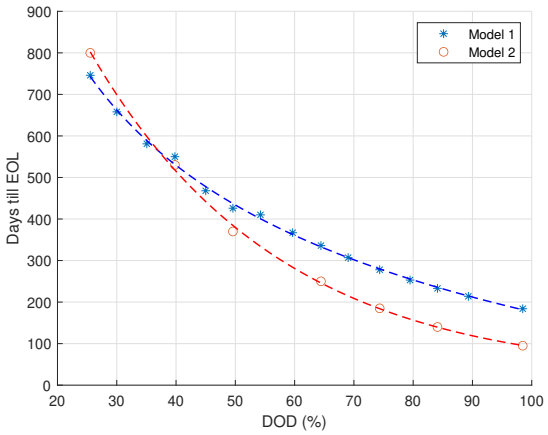

(b) Comparison between NMC Model 1 [63] and Model 2 [31]

Figure 4.1: LFP and NMC aging for Scenario 1 (IMC only)

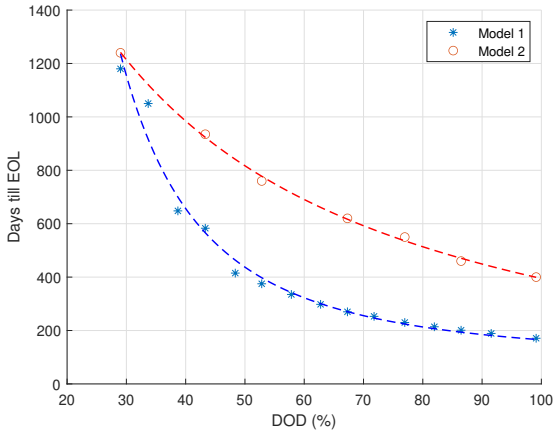

(a) Comparison between LFP Model 1 [62] and Model 2 [31]

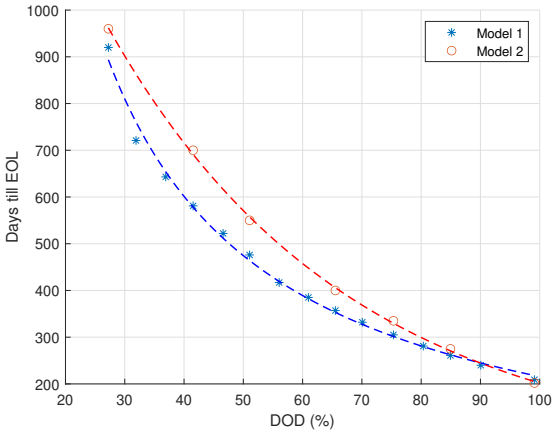

(b) Comparison between NMC Model 1 [63] and Model 2 [31]

Figure 4.2: LFP and NMC aging for Scenario 2 (IMC plus stationary charging at Arnhem Centraal)

In summation, the evaluation of LFP chemistry leads to the assertion that Model 1's reliance on fixed constant values for B_{cyc}, designated for specific cell currents and subsequently extended to interpolate values for intervening current levels, may not provide the most comprehensive and accurate outcomes. This limitation becomes particularly evident when considering the influence of varying current magnitudes on battery aging. The substantial divergence in B_{cyc} values between closely spaced current levels, such as 1A and 1.5A, potentially undermines the reliability of the results. However, it's worth noting that Model 1 does exhibit a degree of effectiveness under conditions characterized by consistently high or low currents, where B_{cyc} values remain relatively stable. In contrast, Model 2's approach, which dynamically considers stress factors relative to a reference, offers a more robust and uniform degradation prediction, capable of accommodating a wider range of operating conditions.

4.2.2. NMC comparison

In the case of NMC batteries, a notable degree of resemblance is observed between both models. Model 1, for NMC batteries, operates on a calendar aging component that remains independent of SOC, and its influence on the overall cyclic aging diminishes as the duration during which the current (I=0) decreases. This effect is particularly in Scenario 2, where a reduction in aging is evident compared to Scenario 1. This

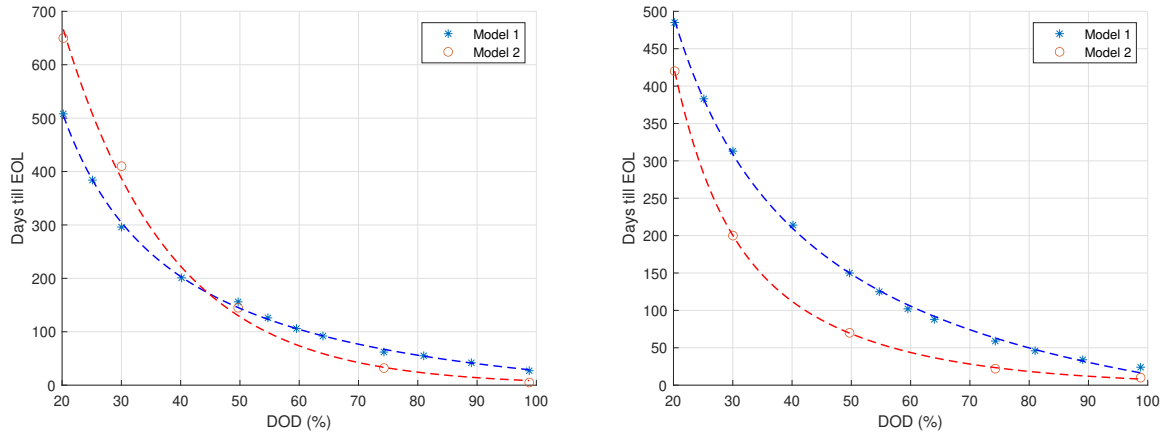

(a) Comparison between LFP Model 1 [62] and Model 2 [31] **(b)** Comparison between NMC Model 1 [63] and Model 2 [31]

Figure 4.3: LFP and NMC aging for Scenario 3 (IMC plus opportunity charging at Wageningen station)

reduction is attributed to the decrease in charging power and subsequently the c-rate, a consequence of the generalized preexponential factor employed in Model 1. The model's design, tailored for c-rates ranging from 0.5C to 6.5C [64], inadvertently underscores its ability to effectively predict aging at exceedingly high c-rates, as is evident in Scenario 3.

Model 2 adheres to an approach based on stress factors and their relative influence concerning a reference condition. As such, Model 2 furnishes a comprehensive and insightful analysis of NMC battery aging across diverse scenarios. The influence of stress factors within both Model 1 and Model 2 is notably more robust and pronounced when compared to Model 1's representation. This heightened emphasis on different stress factors renders this model more comprehensive in nature.

4.3. Battery aging for different charging scenarios

The Open-Sesame battery models were employed as the foundation for comparing battery aging behaviors across different scenarios. The choice of these models was motivated by their comprehensive nature, which enables a thorough investigation of aging dynamics under varying conditions.

Distinct battery sizes were employed for different scenarios, leading to a notable distinction between scenarios 1 and 2 when compared to scenarios 3 and 4. The former scenarios utilized uniform battery sizes, aligned with the consistent energy requirements, while scenario 3 saw the introduction of battery sizes tailored to the reduced energy demands. Scenario 4 on the other hand featured oversized batteries due to overnight charging and reduced charging power under the catenary.

To facilitate a comprehensive comparison, the EOL analysis was conducted by juxtaposing battery size against the anticipated EOL for each of the three battery chemistries: LFP, NMC, and LTO. This comparison provides valuable insights into the varying aging patterns exhibited by these chemistries under different battery sizes and charging scenarios. The resulting battery size vs EOL plots offer a clear visualization of the interactions between battery chemistry, sizing decisions, and operational conditions, shedding light on optimal strategies for enhancing battery lifespan within the intercity IMC bus system.

Scenario 1, requires substantial charging power when connected to the catenary. This exerts an adverse impact on battery aging, attributable to the heightened aging resulting from the battery cells contending with elevated C-rates. Scenario 2 seeks to address this concern by integrating stationary charging during the bus stop at Arnhem Centraal. Notably, despite the increase in the count of charge cycles per trip, Scenario 2 manages to curtail the adverse aging effects observed in Scenario 1. This can be attributed to lower charging powers involved, signifying enhanced battery health and a consequent reduction in aging. This is consistently observed across all three distinct battery chemistries.

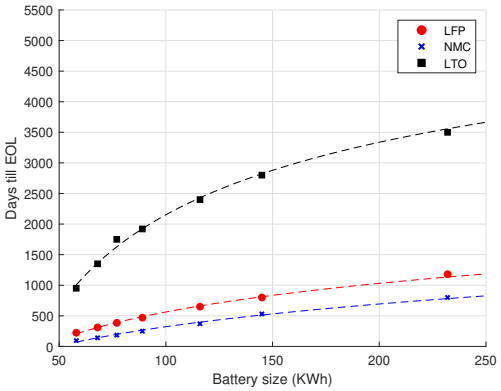

Figure 4.4: Battery Aging for scenario 1 (IMC only)

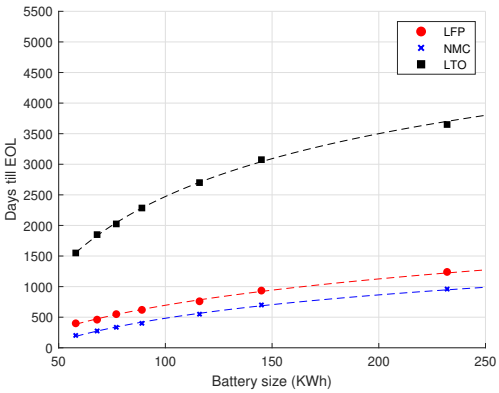

Figure 4.5: Battery Aging for scenario 2 (IMC plus stationary charging at Arnhem Centraal)

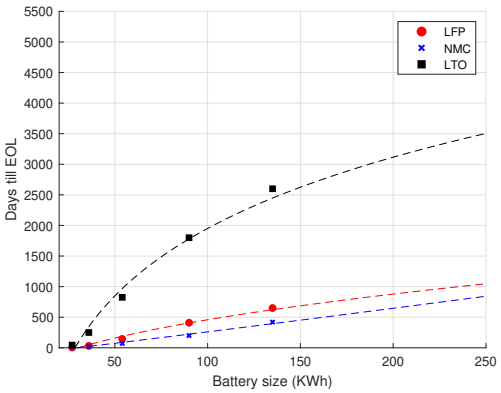

Figure 4.6: Battery Aging for scenario 3 (IMC plus opportunity charging at Wageningen station)

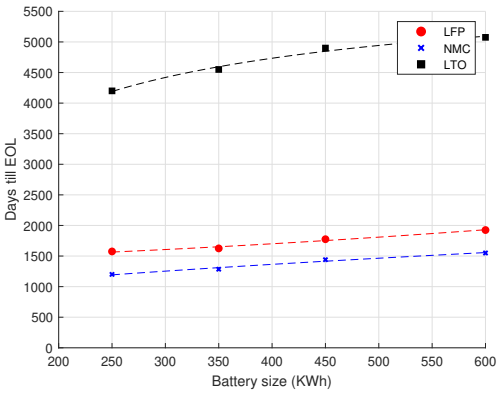

Figure 4.7: Battery Aging for scenario 4 (IMC plus overnight charging at Arnhem Centraal)

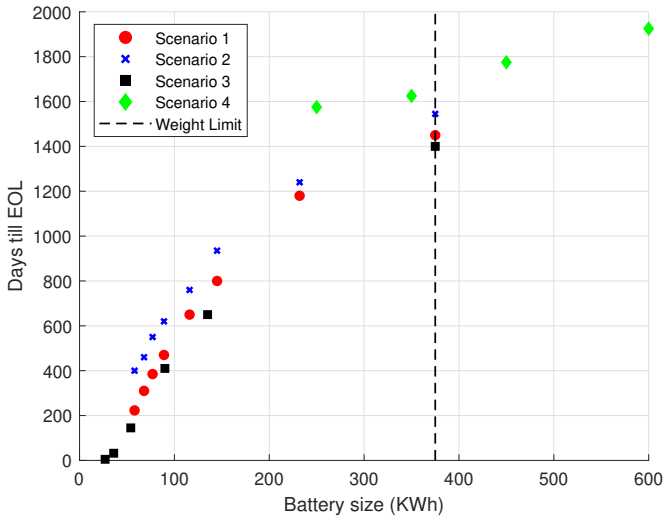

Figure 4.8: LFP battery aging for different charging scenarios

Scenario 3, despite having the lowest charging power under the catenary in comparison to the other scenarios, a contrasting narrative emerges due to the interplay of distinct factors. The high charging power

associated with opportunity charging, coupled with a significant increase in the tally of charge and discharge cycles, collectively exerts an adverse impact on battery aging. All three distinct battery chemistries are significantly affected by this.

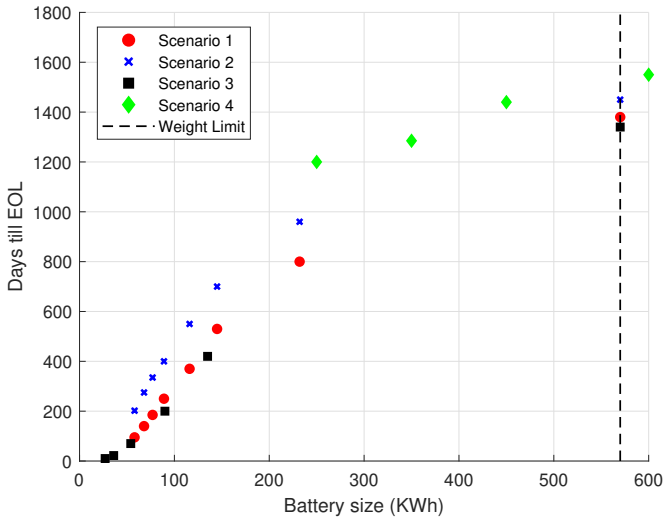

Figure 4.9: NMC battery aging for different charging scenarios

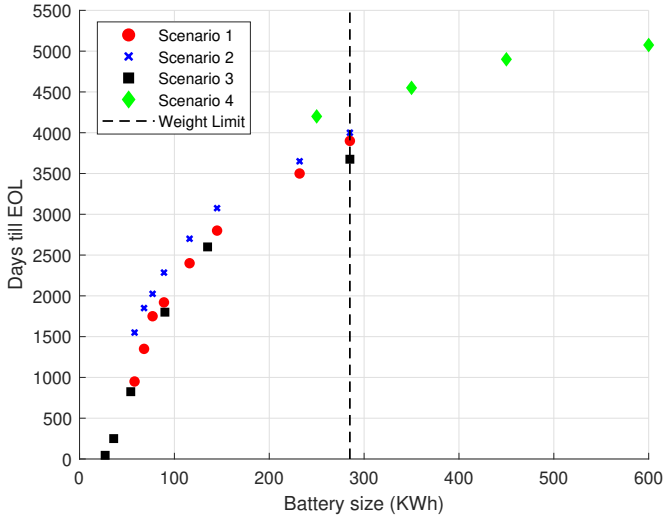

Figure 4.10: LTO battery aging for different charging scenarios

Scenario 4 is characterized by a reduction in catenary charging power and the integration of a larger battery size with an overnight charging system. This configuration results in an appreciable reduction in aging for all three chemistries. The adoption of larger battery size, coupled with the implementation of overnight charging, results in lower C-rates during typical operations, while a decrease in the count of charge and discharge cycles also mitigates aging effects on the battery. The scenario's reliance on lower-power overnight charging emerges as a pivotal contributor, effectively counterbalancing aging-inducing factors present in other scenarios.

The diverse aging outcomes across these scenarios lay the foundation for identifying the optimal solution among them. This crucial analysis is undertaken in the subsequent chapter.

4.4. Summary

This chapter delved into the exploration of battery aging phenomena, focusing on different charging scenarios and battery chemistries, specifically LFP, NMC and LTO. The analysis employed a range of empirical and semi-empirical battery models sourced from existing literature. By comparing these models, valuable insights were obtained regarding their strengths and limitations for different chemistries. Notably, the models derived from Open-Sesame showcased a higher level of comprehensiveness compared to other models. Across all four scenarios, LTO batteries consistently demonstrate superior lifespan when compared to LFP and NMC batteries.

An insightful overview was gained of how various charging scenarios impact battery aging. In Scenario 1, the battery faces substantial charging power from the catenary, leading to accelerated aging due to the elevated C-rates. Scenario 2, in contrast, incorporates stationary charging at Arnhem Centraal, effectively reducing aging effects by employing lower charging powers, across all chemistries. Scenario 3, with the lowest catenary charging power, experiences adverse battery aging due to the combination of high opportunity charging power and increased charge-discharge cycles. However, Scenario 4 adopts a different approach by lowering catenary charging power, integrating larger batteries, and implementing overnight charging. This strategy significantly reduces aging for all chemistries, with lower C-rates during regular operations and fewer charge cycles playing key roles, highlighting the importance of overnight charging in offsetting aging effects.

By examining the simulation results, a foundation was laid for informed decision-making in terms of battery selection and sizing for the intercity IMC bus system. The aging outcomes generated from the Open-Sesame models will serve as a critical input for the subsequent chapter, which delves into the optimization of battery size for the identified charging scenarios.

5

Comparing Battery Solutions

In this chapter, the focus is on utilizing aging data to determine the most suitable battery size and battery chemistry among LFP, NMC, and LTO for each charging scenario considered in the intercity IMC bus system. For each charging scenario, identification of the optimal battery size that balances the requirements of the bus's operational demands, battery lifespan, and overall cost considerations will be carried out with all three battery chemistries. The chapter will culminate in recommendations for selecting the most appropriate battery size and chemistry for each charging scenario.

5.1. Inputs

This section presents the essential input parameters necessary for the optimal battery sizing procedure. These parameters encompass both bus-specific variables and those related to the chosen battery technology. The optimization process hinges upon these inputs, which collectively define the operational context and guide the decision-making framework.

5.1.1. Inputs related to the bus

The energy and power requirement for the journey, denoted as E_{max} and P_{max} respectively, are one of the biggest constraints. These values are derived from the velocity profile and the underlying bus model, which computes the temporal power prerequisites. This was detailed in Chapter 3. Importantly, these energy and power demands are subject to variation depending on the chosen scenario.

Along with the energy and power requirements, several other inputs are required. The anticipated lifespan of the trolleybus, its operational days within a year, and the maximum permissible weight of the battery technology are all necessary components. Furthermore, the daily number of trips significantly influences the number of charge/discharge cycles. These are listed in Table 5.1.

Input	Value
Life expectancy of the bus in years (L_{bus})	15
Working days in a year (NW_{bus})	365
Number of trips in a day (N_{trip})	12
Maximum battery weight in kg (W_{max})	3000

Table 5.1: Input parameters relating to the bus for optimal battery sizing

5.1.2. Inputs related to battery technology

Several key factors, like the energy density, power density, and cost of production are inherent to each battery chemistry. These parameters exhibit distinct variations across different battery chemistries, thereby exerting a significant influence on the choice. The data pertinent to these critical factors has been sourced from various references [65, 66, 67, 68, 69, 70, 22, 71].

The initial costs attributed to batteries encompass engineering costs, battery pack costs, costs associated with power electronics, and expenses incurred for vehicle modifications. It is important to note that the quantification of most of these cost parameters falls beyond the scope of this thesis. The focus of this analysis is specifically confined to the domain of battery pack costs. This concentration is rationalized by the fact that the remaining costs are largely independent of battery lifespan. By limiting the initial costs to the battery pack exclusively, it becomes clear on how much the battery costs during its time in the vehicle without considering the costs related to other parts like power electronics or altering the vehicle, which might last longer than the battery. Nevertheless, when conducting a thorough study of the battery's complete life cycle, these costs should certainly be taken into account.

The cost of the battery technology encompasses a holistic estimation, as it includes raw materials costs, costs associated with manufacturing processes, costs associated with testing protocols, etc. The determination of the cost at the pack level of the battery technology is a significant consideration. This calculation, as per insights from [72], is achieved through the application of a cell-to-pack ratio, which stands at a ratio of between 60:40 to 85:15. In the case of NMC cells, a cell-to-pack ratio of 60:40 was employed, while for LTO cells, a higher cell-to-pack ratio of 85:15 was adopted due to its relatively lower energy density requiring a greater amount of material. As per [16], NMC costs are estimated to be 2 to 3 times lower than LTO costs, and the obtained cost values for these chemistries appear to align with this range. This battery pack not only contains the costs associated with the cells but also the accessories like safety, wiring, mountings, etc. This ratio serves as a determinant to calculate the total cost of the battery pack [72, 16, 73]. Table 5.2 lists the battery characteristics.

Battery chemistry	Energy density	Power density	Cost per kWh
LFP	125 Wh/kg	800 W/kg [48]	200 [73]
NMC	190 Wh/kg	1100 W/kg [71]	240 [73]
LTO	90 Wh/kg [22]	2200 W/kg [22]	585 [16]

Table 5.2: Battery characteristics for optimal battery sizing

This optimal sizing procedure does not rely on generic data representations for battery aging, such as fixed cycle numbers corresponding to specific battery chemistries. The optimization process herein is underpinned by a scenario-specific approach, harnessing aging data tailored to the specific operational scenarios under consideration. This was done by the execution of battery aging simulations based on semi-empirical models as extensively reviewed in Chapter 4.

5.2. Optimal battery sizing procedure

The optimization procedure can be divided into several steps.

Step 1: Input Parameters

The first step involves the input parameters, which serve as fundamental criteria for assessing and finding the optimal battery size for integration with trolleybuses.

These include :

- E_{max}: The desired energy requirement in kilowatt-hours (kWh) for the battery system.
- P_{max}: The specified power requirement in kilowatts (kW) for the battery system.
- L_{bus}: The anticipated operational lifespan of the trolley bus in years.
- NW_{bus}: The number of working days the bus operates in a year.
- W_{max}: The maximum permissible weight of the battery system on the trolley bus in kilograms (kg).
- N_{trip}: The number of bus trips per day.
- sp_{E}: The energy density in kWh/kg for the battery system.
- sp_{p}: The specific power in kW/kg for the battery system.
- C_{p}: The production cost per kWh.

Step 2: Optimization Loop

This step encompasses an iterative process for assessing the suitability of different battery system configurations based on varying weights, addressing the energy and power requirements.

The loop initializes the weight of the battery system,W_{bs}, at a percent of the maximum allowable weight (W_{max}). It calculates the corresponding energy (E_{bs}) based on the energy density of the selected battery technology. The loop considers whether the selected battery system can meet energy requirements, ensuring E_{bs} exceed the maximum energy requirements E_{max}. The loop calculates the DoD and retrieves the number of cycles (N_{c1}) data from an external source using a look-up table based on results from Chapter 4 which then gives the life of the battery (L_{bs}). The number of battery replacements (k) is then calculated from L_{bus} and L_{bs}. Eligible battery system configurations are stored in arrays for further analysis.

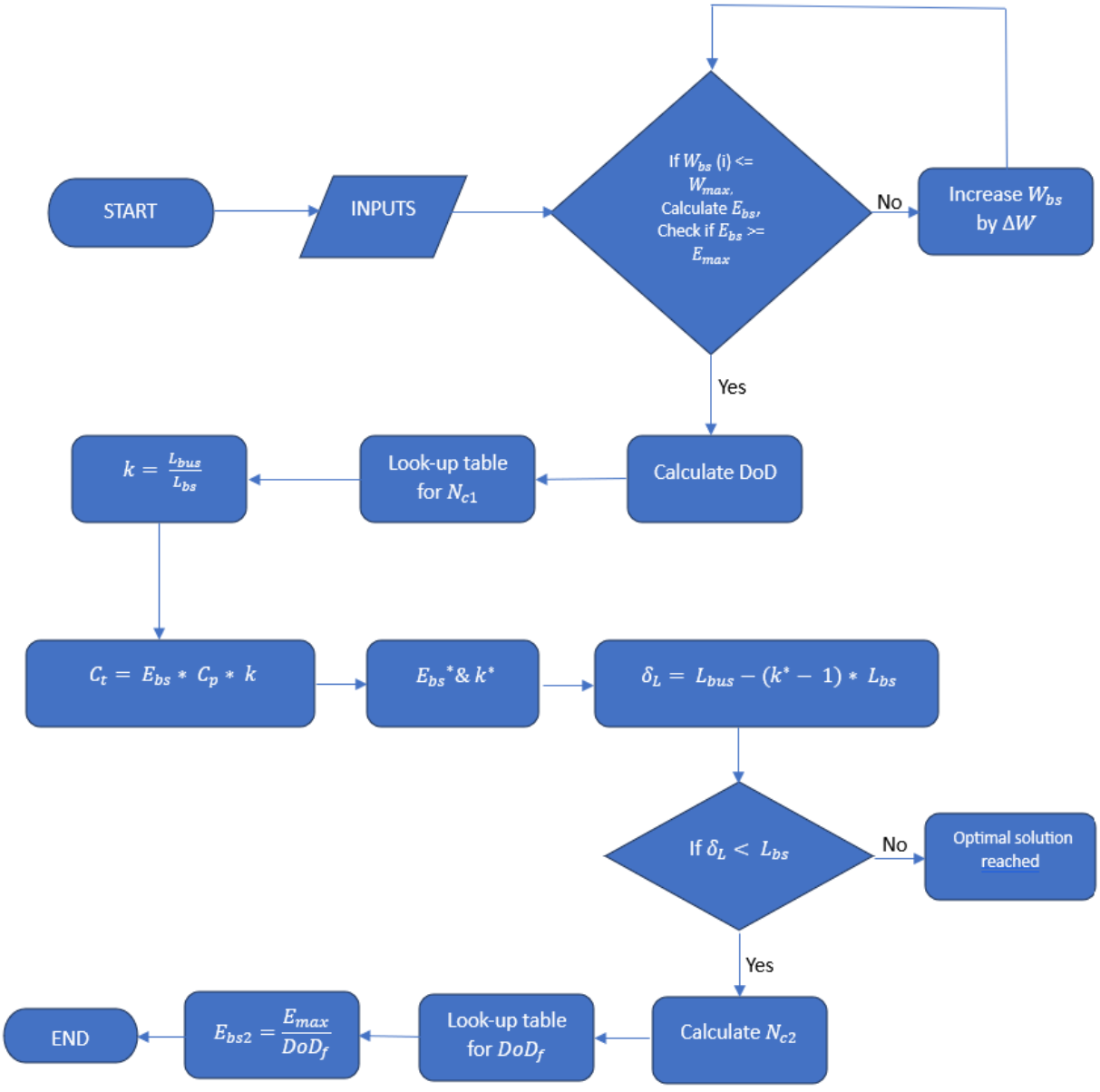

Figure 5.1: Optimal battery sizing based on aging data, cost of production, and weight constraints

Step 3: Configuration Analysis

This step involves analyzing the array of potential battery system configurations to determine the optimal solution considering factors such as cycle life, energy capacity, and cost-effectiveness.

First the battery system with the lowest cost (C_{t}), which factors in cycle life, production cost (C_{p}), and number of replacements (k). Corresponding cycle-life values (L_{bs}), energy capacity (E_{bs}), and DoD are retrieved for the optimal configuration E^*_{bs} and k^* is the number of replacements required. Then the remaining operational lifespan (δ_{L}) for the last battery system on the trolley bus is calculated.

If the remaining lifespan permits, the script calculates a new cycle-life (N_{c2}) to accommodate the remaining operational period and adjusts energy capacity accordingly, E_{bs2}, by increasing the DoD requirement to DoD_{f}. This results in optimal battery system specifications, encompassing weight, cycle life, energy capacity, depth of discharge, and cost.

Step 4: Cost Analysis and Savings

This step involves quantifying the cost implications of different battery system configurations and determining potential cost savings. The total cost for two scenarios, one without optimizing the last battery size and the other with optimizing the last battery size is calculated, reflecting adjusted energy capacity and cycle-life for the last replacement. Cost savings resulting from adopting the case of reducing the last battery size are quantified.

This battery sizing methodology offers a holistic understanding of the battery system optimization process, emphasizing the importance of balancing energy, cycle life, and cost considerations to achieve a cost-effective IMC bus system.

5.3. Results

In this section, the practical application of the previously outlined procedure to real-world case scenarios is examined. In the optimization procedure, the initial battery system weight remains set at five percent of the maximum allowable weight. The procedure subsequently generates all eligible battery sizes that fulfill the energy and power requirements. For each battery size, the calculation of replacements is based on battery life derived from the aging data. This process enables the selection of an optimal battery size for each scenario, considering the costs associated with battery aging and replacements.

The optimization results are presented through Figures 5.2 to 5.13. These include all the four scenarios previously described Chapter 3. For a recap, scenario 1 is of IMC charging only, scenario 2 is of IMC plus stationary charging at Arnhem, scenario 3 is IMC plus opportunity charging at Wageningen and the final scenario is IMC charging with overnight charging at depot (Arnhem Centraal).

Within scenarios 1 and 2, where the minimum energy requirement stands at 58 kWh, it is noteworthy that batteries possessing a capacity of 58 kWh adequately fulfill both the energy and the power requirement of 300 kW. However, in scenario 3, characterized by an energy requirement of 27 kWh, NMC batteries nearing 50 kWh manifest the ability to satisfy both energy and power requirements. This phenomenon arises from the relatively low specific power inherent to NMC batteries in contrast to LFP and LTO counterparts, allowing these batteries to fulfill the required criteria within a smaller battery size.

Moving to Figures 5.2, 5.5, 5.8, 5.11 a depiction of battery replacements for varying battery sizes across all three chemistries is provided. This representation shows the battery life disparities among the chemistries. LTO batteries exhibit the longest lifespan, thus requiring the fewest replacements across different sizes. Following this, LFP batteries necessitate replacements in a greater frequency, while NMC batteries manifest the shortest lifespan, leading to comparatively higher replacement frequencies. With the increase in battery size, the number of replacements decreases or remains constant. In scenarios 1, 2, and 3, particularly concerning LFP and NMC batteries, their diminished longevity at lower battery capacities necessitates an impractical frequency of replacements.

In Figures 5.3, 5.6, 5.9, 5.12 a correlation is depicted between the number of replacements and the utilization of higher DoD levels in battery operation. As DoD utilization increases, there is a reduction in the frequency of replacements required.

In Figures 5.4, 5.7, 5.10, 5.13 the total cost associated with a specific battery size is presented. This cost captures not only the cost for individual battery systems but also considers the collective costs incurred for deploying all required replacement units, ensuring coverage for the desired operational lifespan. It's important to recognize that while the cost of a single battery system increases with its size, the

aggregate cost of all replacements together could exhibit a different trajectory depending on the frequency of replacements.

With the expansion of battery size, a noteworthy phenomenon unfolds: the fixed energy requirement leads to a reduction in the DoD with an increase in battery size. This resultant decrease in DoD results in a positive impact on the aging of the battery, translating to an increase in the number of cycles the battery can undergo. This increased cycling capacity contributes to battery longevity. However, a correlation emerges, where an extension in the battery system's useful life does not universally culminate in a lower cost. This is because the number of replacements remains the same. In instances where the increase in battery capacity fails to yield a proportionate increase in its useful life, the reduction in replacement remains the same despite larger battery sizes. Consequently, while the number of replacements remains the same despite increasing the battery size, the overall cost of the battery system experiences an increase. As the battery size increases, total cost trends downward exclusively when the reduction in replacement expenses (attributed to prolonged battery life) surpasses the cost escalation attributed to substituting larger-capacity batteries. This delicate balance between replacement-related cost reduction and the expenditure associated with higher-capacity battery integration significantly influences the economic implications of increasing the battery size.

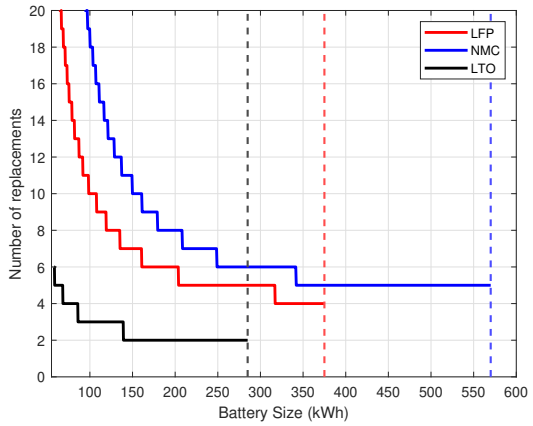

Figure 5.2: Battery size (kWh) vs replacements for scenario 1 (IMC only)

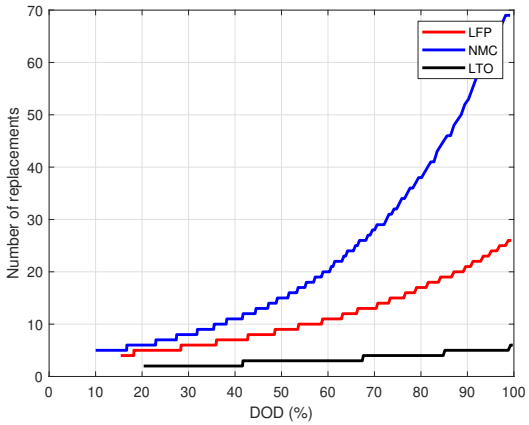

Figure 5.3: Replacements vs DoD for scenario 1 (IMC only)

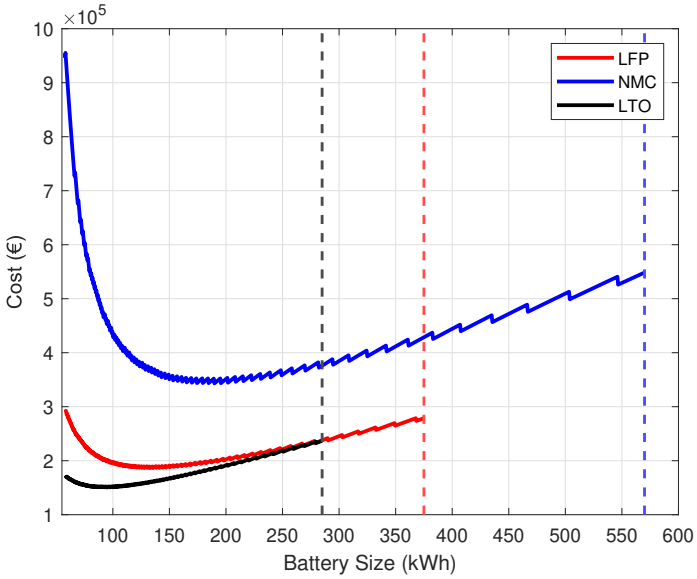

Figure 5.4: Battery size (kWh) vs cost(€) for scenario 1 (IMC only)

	LFP	NMC	LTO
Weight of the smallest battery (kg)	1056	1000	1000
Number of replacements	8	8	3
Size (kWh)	132	190	95
Max DoD (%)	43.54	30.08	60.93
Battery life (years)	2.14	1.99	5.55
Last battery size (kWh)	58	115	70
Max DoD of last battery (%)	98.84%	49.32%	83.10%
Total cost in € (case 1)	211200	364800	166725
Total cost in € (case 2)	196400	346800	152100
Savings (€)	14800	18000	14625

Table 5.3: Optimal parameters for the battery for scenario 1 (IMC only)

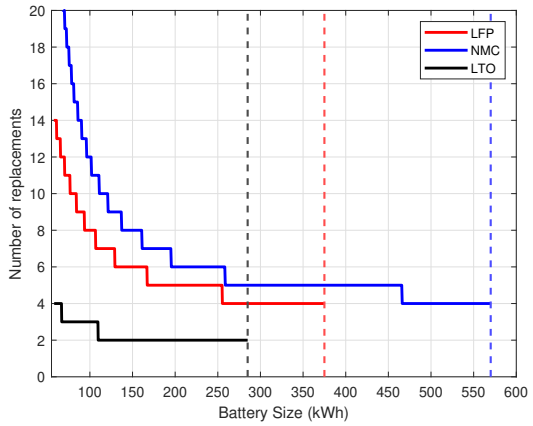

Figure 5.5: Battery size (kWh) vs replacements for scenario 2 (IMC plus stationary charging at Arnhem Centraal)

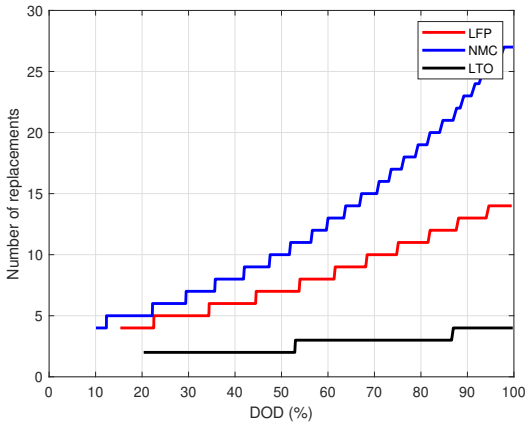

Figure 5.6: Replacements vs DoD for scenario 2 (IMC plus stationary charging at Arnhem Centraal)

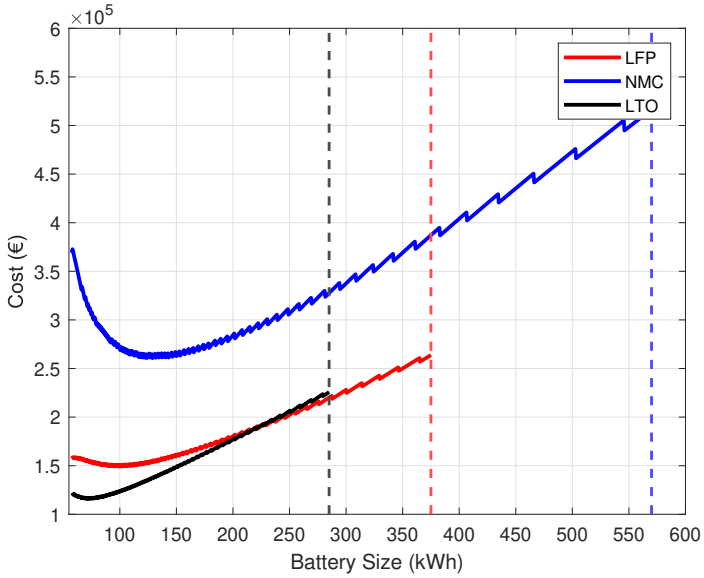

Figure 5.7: Battery size (kWh) vs cost(€) for scenario 2 (IMC plus stationary charging at Arnhem Centraal)

	LFP	NMC	LTO
Weight of the smallest battery (kg)	792	674	758
Number of replacements	8	9	3
Size (kWh)	99	128	72
Max DoD (%)	58	45	81
Battery life (years)	1.99	1.78	5.42
Last battery size (kWh)	58	69	58
Max DoD of last battery (%)	99	84	100
Total cost in € (case 1)	158400	276480	126360
Total cost in € (case 2)	150200	262320	118170
Savings (€)	8200	14160	8190

Table 5.4: Optimal parameters for the battery for scenario 2 (IMC plus stationary charging at Arnhem Centraal)

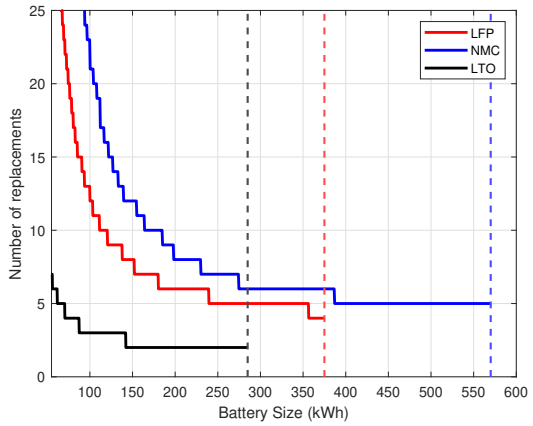

Figure 5.8: Battery size (kWh) vs replacements for scenario 3 (IMC plus opportunity charging at Wageningen station)

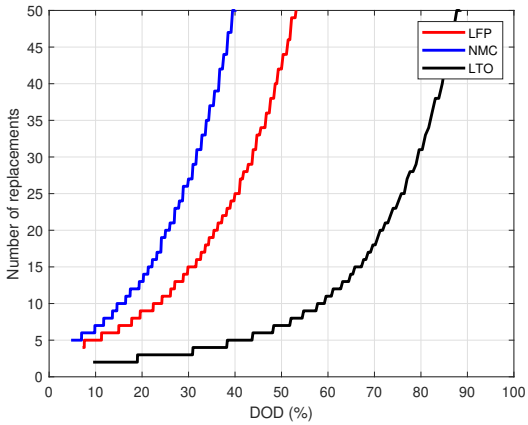

Figure 5.9: Replacements vs DoD for scenario 3 (IMC plus opportunity charging at Wageningen station)

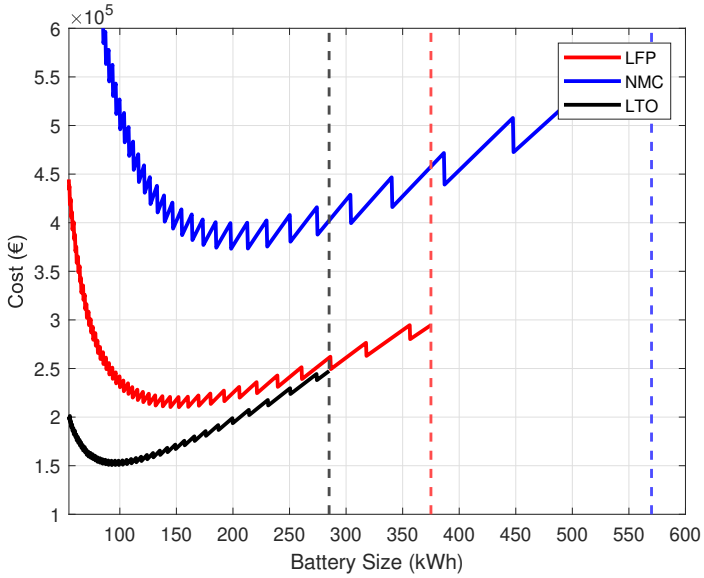

Figure 5.10: Battery size (kWh) vs cost(€) for scenario 3 (IMC plus opportunity charging at Wageningen station)

	LFP	NMC	LTO
Weight of the smallest battery (kg)	1216	1042	968
Number of replacements	7	8	3
Size (kWh)	152	198	92
Max DoD (%)	17.73	13.61	29
Battery life (years)	2.17	1.91	5.41
Last battery size (kWh)	140	180	75
Max DoD of last battery (%)	19.15	15.07	35.94
Total cost in € (case 1)	212800	380160	161460
Total cost in € (case 2)	210400	375840	151515
Savings (€)	2400	4320	9945

Table 5.5: Optimal parameters for the battery for scenario 3 (IMC plus opportunity charging at Wageningen station)

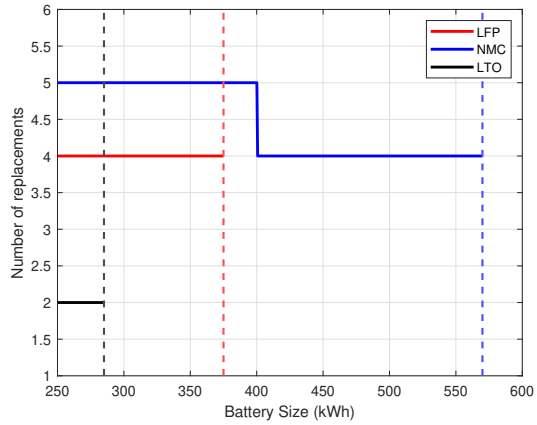

Figure 5.11: Battery size (kWh) vs replacements for scenario 4 (IMC plus overnight charging at Arnhem Centraal)

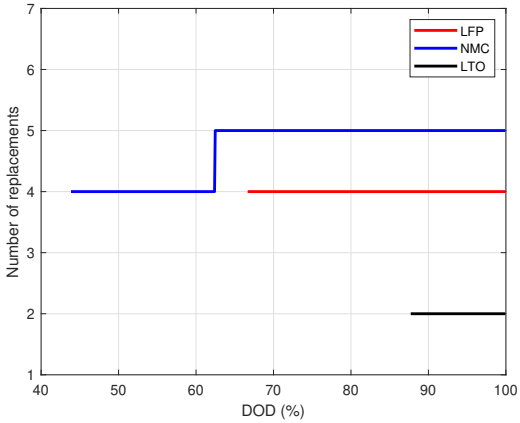

Figure 5.12: Replacements vs DoD for scenario 4 (IMC plus overnight charging at Arnhem Centraal)

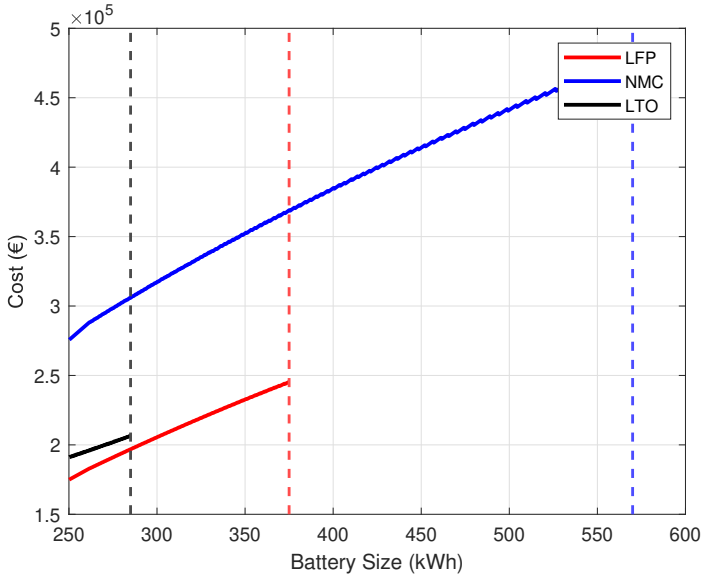

Figure 5.13: Battery size (kWh) vs cost(€) for scenario 4 (IMC plus overnight charging at Arnhem Centraal)

	LFP	NMC	LTO
Weight of the smallest battery (kg)	2000	1315	2631
Number of replacements	4	5	2
Size (kWh)	250	250	250
Max DoD (%)	98	95	100
Battery life (years)	4.29	3.27	11.48
Last battery size (kWh)	-	-	-
Max DoD of last battery (%)	-	-	-
Total cost in € (case 1)	200000	300000	292500
Total cost in € (case 2)	-	-	-
Savings (€)	-	-	-

Table 5.6: Optimal parameters for the battery for scenario 4 (IMC plus overnight charging at Arnhem Centraal)

The optimal battery sizes along with the least cost associated with the battery sizes are listed in Tables 5.3, 5.4, 5.5, 5.6.

- Scenario 1:

  The consideration of weight assumes a critical role in the selection of batteries. In the current scenario, LTO batteries exhibit a weight of 1000 kg, as opposed to the LFP (1056 kg) and NMC (1000 kg) counterparts. While this difference in weight is relatively modest, it implies that other factors could potentially counterbalance this distinction.

  Upon closer examination of the three distinct battery chemistries, it becomes evident that LTO offers the smallest battery capacity, operating at a higher DoD of 60.93%, in comparison to LFP and NMC batteries with capacities of 132 kWh and 190 kWh, operating at DoDs of 43.54% and 30.08%, respectively. The estimated battery life for LFP and NMC stands at 2.14 years and 1.99 years, respectively. In this scenario, LTO emerges as the clear frontrunner, having a longer battery life of 5.55 years. This prolonged lifespan translates into a reduced frequency of replacements, thereby exerting a positive influence on minimizing the overall battery system costs throughout the operational span of 15 years.

  One of the most critical aspects of battery performance is the overall costs, encompassing elements such as the initial battery cost and subsequent replacement costs. Specifically, LFP batteries entail a total cost of €211,200, NMC batteries amount to €364,800, and LTO batteries offer the most economically efficient solution with a total cost of €166,725.

  The approach of adjusting the size of the last battery to a smaller value, while concurrently operating it at a higher DoD, can yield significant cost savings. This effect is particularly pronounced in LTO batteries, which lead in terms of savings, amounting to €14,625 (8.78% of the total cost in case 1). Similarly, LFP and NMC batteries demonstrate savings of €14,800 (7.00%) and €18,000 (4.9%), respectively. These figures underscore the substantial financial benefits associated with optimizing the size of the last battery, contingent on the remaining operational life of the trolley bus.

- Scenario 2: LFP batteries showcase a weight of 792 kg, whereas NMC batteries demonstrate a slightly lighter weight of 674 kg. In contrast, LTO batteries register a weight of 758 kg. While LFP batteries appear the heaviest, the differences between the three types are relatively modest, suggesting that other influential factors need consideration.

  Considering battery size and characteristics, LFP batteries with a capacity of 99 kWh (operating at a DoD of 58%) are projected to have a battery life of 1.99 years. In contrast, NMC batteries possess a larger capacity of 128 kWh (operating at a DoD of 45%), yet exhibit a slightly shorter battery life of 1.78 years. Intriguingly, LTO batteries feature the smallest capacity, amounting to 72 kWh, and operate at a higher DoD of 81%, resulting in a battery life of 5.42 years.

  A noteworthy observation is that LFP and NMC batteries require 8 and 9 replacements, respectively, throughout their operational lifespan, whereas LTO batteries demand only 3 replacements. This

disparity in replacement frequency underscores the distinct lifecycle characteristics inherent to each battery type.

From a cost perspective, LFP batteries entail a total expenditure of €150,200, while NMC batteries amount to €262,320. Conversely, LTO batteries emerge as the most economically viable solution, a total cost of €118,170. By optimizing the size of the final battery, significant savings can be achieved. Specifically, for LFP batteries, a savings of approximately 5.18% is realized, while NMC batteries yield a saving of 5.12%. The optimization of LTO batteries results in savings of approximately 6.5%.

- Scenario 3: LFP batteries showcase a weight of 1216 kg, while NMC batteries exhibit a slightly lighter weight of 1042 kg. Comparatively, LTO batteries register a weight of 968 kg.

  LFP batteries, with a capacity of 152 kWh and a DoD of 17.73%, are projected to offer a battery life of approximately 2.17 years. Conversely, NMC batteries, featuring a larger capacity of 198 kWh and operating at a DoD of 13.61%, exhibit a slightly shorter battery life of around 1.91 years. Intriguingly, LTO batteries, with a capacity of 92 kWh and a higher DoD of 29%, show an impressive battery life of 5.41 years. This situation highlights the importance of operating batteries at DoD levels to ensure their optimal health. The reason for this recommendation is the frequent daily charge-discharge cycles that the battery experiences. By reducing the DoD, the battery's overall lifespan can be extended effectively which makes this scenario competitive to other scenarios.

  LFP batteries necessitate 7 replacements over their operational lifespan, while NMC batteries call for 8 replacements, whereas LTO batteries outperform both counterparts, requiring only 3 replacements.

  LFP batteries entail a total expenditure of €212,800, whereas NMC batteries command a higher cost of €380,160. LTO batteries emerge as the most economically viable option, with a total cost of €161,460. Notably, savings can be attained by optimizing the size of the final battery configuration. LFP batteries yield savings of approximately 1.12%. NMC batteries of approximately 1.13%, whereas LTO batteries yield savings of approximately 6.16%.

- Scenario 4:

  The LFP battery weight registered at 2000 kg. Comparatively, the NMC battery boasts a weight of 1315 kg, while the LTO battery showcases the heaviest weight among the three, at 2631 kg. This is due to the fact that for all three battery chemistries, the optimized battery size is the same, which is 250 kWh, operating at close to 100% DoD. This weight difference is significant due to the difference in their specific energy values.

  LFP batteries demand only 4 replacements, while NMC batteries require 5 replacements. Impressively, LTO batteries stand out with an even lower replacement frequency, necessitating only 2 replacements. LFP batteries are projected to offer a battery life of approximately 4.29 years, while NMC batteries exhibit a slightly shorter battery life of about 3.27 years. Strikingly, LTO batteries exhibit a remarkable battery life of 11.48 years.

  In the case of LFP batteries, a total cost of €200,000 is incurred, NMC batteries amount to €300,000, and LTO batteries amount to a total cost of €292,500. This high cost of LTO can be attributed to the fact that, despite its impressive battery life of 11.48 years, a 250 kWh battery is still required to adequately fulfill the operational demands of this specific scenario. It is pertinent to mention that in each of the three battery chemistries, the optimal solution is the lowest capacity battery, which, eliminates the need for further optimization of the final battery size.

5.4. Scenario comparison

In the preceding section, the analysis focused on calculating the costs of battery systems over the entire operational lifespan of various scenarios. This provided valuable insights into identifying the most suitable battery chemistry for each scenario. However, these calculations solely encompassed the battery costs and did not account for the expenses associated with the required charging infrastructure. While scenarios 1, 2, and 4 benefited from the existing trolley grid infrastructure at Arnhem for in-motion charging, stationary charging, and overnight charging respectively, scenario 3 necessitates the installation of an opportunity charger. Additionally, in order to arrive at a comprehensive estimate, the vehicle cost should also be taken into consideration, taking into account all the components associated with each scenario.

Parameter	Value
Vehicle cost	€350000
Fleet size	9
Service life of vehicle	15 years
Fast charger cost	€250000
Yearly charging device maintenance	3%
Service life of charging device	20 years

Table 5.7: Cost parameters [74]

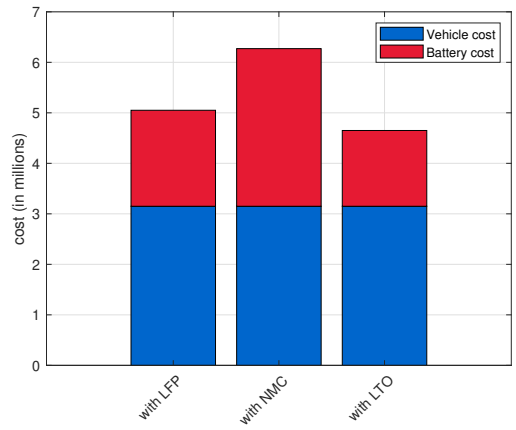

Figure 5.14: Cost for Scenario 1 (IMC only)

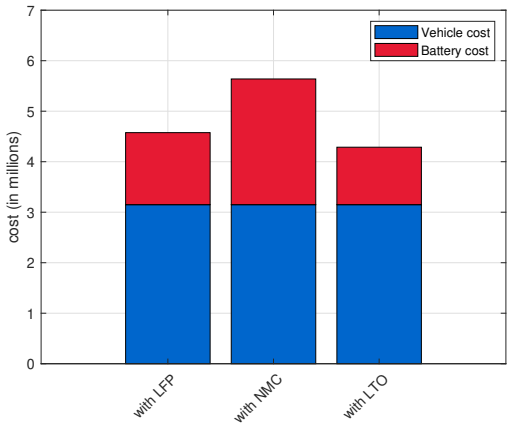

Figure 5.15: Cost for Scenario 2 (IMC plus stationary charging at Arnhem Centraal)

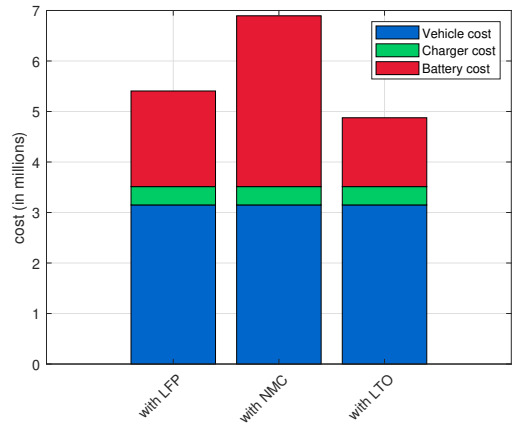

Figure 5.16: Cost for Scenario 3 (IMC plus opportunity charging at Wageningen station)

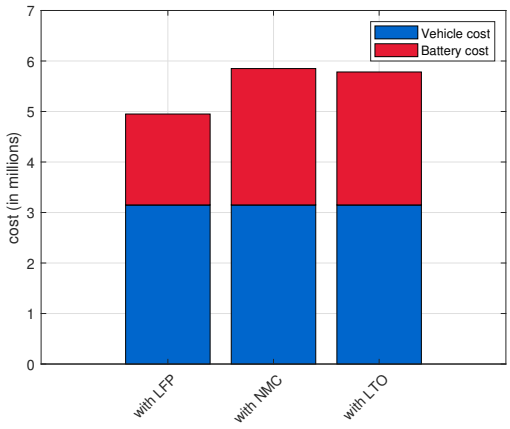

Figure 5.17: Cost for Scenario 4 (IMC plus overnight charging at Arnhem Centraal)

Figures 5.14 through 5.17 present the total costs associated with each respective scenario. Scenarios 1, 2, and 4 stand to benefit from existing infrastructure, contributing to their reduced costs when compared to scenario 3. The findings suggest that Scenario 2 emerges as the most economical solution among the evaluated scenarios. This outcome can be attributed to the advantageous combination of low charging power under the catenary and the implementation of low-power charging at Arnhem Centraal between trips, effectively extending battery life and minimizing replacement requirements. Across the different scenarios and battery chemistries, LTO-based batteries demonstrate the most cost-effective performance within the context of scenario 2 costing €4.28M.

5.5. Summary

This chapter centered on the optimization of battery size, a process necessitating the integration of different input parameters, primarily derived from the findings presented in Chapter 3 and Chapter 4.

LTO batteries consistently outshine LFP and NMC batteries across these scenarios. In Scenario 1, LTO batteries of 95 kWh, exhibit a substantially longer lifespan of 5.55 years compared to LFP (2.14 years) and NMC (1.99 years). This longevity translates into reduced replacement frequency and a lower overall system cost of €166,725, outperforming LFP (€211,200) and NMC (€364,800). In Scenario 2, LTO batteries again excel with a lifespan of 5.42 years, compared to LFP (1.99 years) and NMC (1.78 years). LTO batteries with a size of 72 kWh outshine in both lifespan and cost efficiency with a total cost of €126,360, making them the most economical choice. Scenario 3 demonstrates the cost-effectiveness of LTO batteries of 92 kWh, with a lifespan of 5.41 years, while LFP (2.17 years) and NMC (1.91 years) fall short. LTO batteries, with a total cost of €161,460, surpass LFP (€212,800) and NMC (€380,160) in economic viability. Lastly, in Scenario 4, LTO batteries of 250 kWh, exhibit a remarkable lifespan of 11.48 years, outperforming LFP (4.29 years) and NMC (3.27 years) of the same capacity. LFP with a cost of €200,000, comes out to be the most economical option.

The combination of battery-specific inputs, coupled with bus-related variables, facilitated an effective optimization procedure. This methodology was employed to address four distinct battery usage scenarios. Notably, the comprehensive nature of this approach results from the fact that each scenario entailed its own distinctive aging data specific to each battery chemistry. The outcomes thus obtained represent optimized battery solutions tailored to the requirements of individual scenarios.

6

Conclusion and future works

In this chapter, the thesis findings are summarized through the conclusions drawn from the research questions, presented in section 6.1. Additionally, section 6.2 offers recommendations for future research works.

6.1. Conclusion

1. How can distinct battery load profiles be developed in inter-city IMC buses for varying charging scenarios?

The development of a dynamic bus model capable of generating power traction beyond the catenary network and the incorporation of auxiliary power considerations represented key advancements in understanding the system's total power requirements. The incorporation of IMC occurs primarily under the catenary system. Additionally, alternative charging methodologies, including stationary charging, overnight charging at the Arnhem station, and opportunity charging at Wageningen, are employed along with IMC, resulting in the formulation of four distinct charging scenarios.

With the introduction of in-motion charging in scenario 1, the required charging power under the catenary becomes crucial for the battery to meet operational demands. Different charging powers were explored, and a charging power of 195 kW was found to be sufficient. In order to reduce the charging power under the catenary, the subsequent integration of a stationary charging system of 60 kW at Arnhem Central demonstrated the potential to reduce catenary charging power to 125 kW, leading to potential improvement in battery health. The exploration of opportunity charging 200 kW at Wageningen Central allowed a reduction of catenary charging power to 100 kW. Additionally, the incorporation of overnight depot charging of 50 kW alongside in-motion charging also results in lowering the catenary charging power to 125 kW.

It's crucial to highlight the limitations encountered while addressing this research question. Firstly, the bus model relies on accounting for various forces acting on the vehicle, yet it neglects the consideration of gravitational force. This is primarily due to the generally flat terrain of the Netherlands, but incorporating gravitational force into the model could provide a more comprehensive analysis. Furthermore, the velocity profiles generated outside the catenary system are based on data regarding the bus's top speed and acceleration, which are derived from the velocity profiles observed under the catenary. This approach results in a trapezoidal velocity profile. This profile does not account for velocity fluctuations caused by external factors such as traffic delays or stops. To enhance the accuracy of the velocity profile, either a more sophisticated modeling technique for generating velocity profiles should be employed, or actual velocity data should be measured under real-world conditions. This would allow for a more precise representation of the bus's velocity behavior in various scenarios.

2. What is the comparative effect of various charging scenarios on the aging of commonly employed battery chemistries in IMC vehicles?

The comparison of battery aging behaviors across different scenarios using the Open-Sesame battery models has provided valuable insights into optimal battery sizing and operational strategies for the intercity IMC bus system. The choice of these comprehensive models enabled a detailed exploration of aging

dynamics under diverse conditions. The utilization of distinct battery sizes for various scenarios highlighted the significance of sizing decisions in different operational contexts.

When analyzing the results, it becomes evident that each scenario has distinct implications for battery aging. In Scenario 1, where the battery charging is done solely during in-motion, the requirement for high charging power under the catenary leads to detrimental aging effects due to elevated C-rates. Scenario 2 presents a successful mitigation strategy by incorporating stationary charging at Arnhem along with IMC, effectively reducing aging through lower charging powers. Scenario 3, despite featuring a lower catenary charging power of 100 kW, experiences accelerated aging due to a high charging power of 200 kW during opportunity charging and an increased number of charge/discharge cycles. In contrast, Scenario 4's reduction in catenary charging power to 125 kW, coupled with overnight charging and larger battery sizes (250 kWh and more), leads to reduced aging across all battery chemistries. The adoption of larger batteries with overnight charging contributes to lower c-rates counteracting aging effects.

Collectively, these findings underscore the importance of considering charging strategies and battery sizing together to optimize battery aging. Scenario 4 stands out as particularly promising, as it showcases reduced aging for all battery chemistries. This analysis contributes valuable insights towards making informed decisions about battery selection and sizing, ultimately enhancing the lifespan and cost-effectiveness of battery systems within the intercity IMC bus context.

3. How do different traction battery solutions compare in the context of inter-city IMC buses?

The examination of the four distinct scenarios in conjunction with different battery chemistries yields significant insights into their respective performances. In Scenario 1, the supremacy of LTO batteries becomes evident, due to their smaller capacity and higher operating DoD, resulting in an extended battery life and fewer replacements. This trend persists in Scenario 2, where LTO batteries again stand out, capitalizing on their smaller size and higher DoD to achieve the least cost in comparison to their counterparts through reduced replacements. Similarly, in Scenario 3, LTO batteries shine, propelled by their higher DoD and smaller capacity, leading to prolonged battery life and lower costs. In scenario 4, where LTO batteries, exhibit remarkable longevity, and fewer replacements, but turn out to be more expensive than LFP batteries. Across all scenarios, LTO batteries consistently outperform LFP and NMC counterparts except for scenario 4, demonstrating superior aging characteristics and cost-effectiveness. Consequently, these results collectively advocate for LTO batteries as the optimal choice for the intercity trolleybus system, underlining their extended battery life, reduced replacement frequency, and overall viability as the preferred battery chemistry for IMC bus systems.

Within the scope of this analysis encompassing four distinct scenarios and three diverse battery technologies, Scenario 2, involving IMC with stationary charging at Arnhem using LTO batteries, emerges as the most cost-effective choice. For a fleet size comprising nine buses, the cost of implementing Scenario 2 amounts to €4.28 million. This cost encompasses various aspects, including the initial investment in batteries, battery replacement costs, and vehicle costs.

Nevertheless, the cost estimation for each scenario currently encompasses the upfront costs of batteries, replacement batteries, vehicle costs, and opportunity charger costs. Notably, the cost of the existing IMC infrastructure has not been factored in, as it represents an established structure in this context. To provide a more comprehensive and forward-looking perspective, it would be beneficial to incorporate potential changes in battery prices, given that battery costs tend to fluctuate over time due to increased production capacity and technological advancements.

6.2. Future work

- **Enhanced Velocity Profiles:** To further refine the accuracy of the dynamic bus model, future research should consider incorporating gravitational forces, which, although often negligible on flat terrain like the Netherlands, can provide a more comprehensive analysis. Additionally, utilizing more advanced modeling techniques or collecting real-world velocity data could lead to more precise velocity profiles that account for fluctuations caused by traffic delays or stops.
- **Battery Aging Models:** Expanding the study of battery aging models and their applicability to IMC buses could provide deeper insights. Research on refining these models or developing new ones

tailored specifically to IMC systems would be valuable. Additionally, conducting physical testing and validation of these models under real-world IMC conditions can enhance their accuracy.

- **Battery Future Prices:** Given the fluctuating nature of battery prices, incorporating predictive models for future battery costs into the analysis would provide a more forward-looking cost estimation. This would involve considering how battery costs may change over time due to factors like increased production capacity and technological advancements.
- **Holistic Cost Analysis:** Future studies should aim for a more comprehensive cost analysis that includes all relevant factors. This entails accounting for the cost of the existing IMC infrastructure, as well as evaluating potential savings or costs associated with infrastructure upgrades or modifications to accommodate different charging scenarios.
- **Environmental Impact Assessment:** Consideration of the environmental impact, such as carbon emissions and energy consumption, associated with each charging scenario and battery chemistry could provide valuable insights for sustainable decision-making.

References

[1] European Environment Agency. *Greenhouse gas emissions from transport in Europe*. European Environment Agency, 2019. URL: https://www.eea.europa.eu/data-and-maps/indicators/transport-emissions-of-greenhouse-gases/transport-emissions-of-greenhouse-gases-12.

[2] European Environment Agency. *Greenhouse gas emissions from transport in Europe*. www.eea.europa.eu, Nov. 2021. URL: https://www.eea.europa.eu/ims/greenhouse-gas-emissions-from-transport.

[3] Michael Glotz-Richter et al. "Electrification of Public Transport in Cities (Horizon 2020 ELIPTIC Project)". In: *Transportation Research Procedia* 14 (2016). Transport Research Arena TRA2016, pp. 2614–2619. DOI: https://doi.org/10.1016/j.trpro.2016.05.416. URL: https://www.sciencedirect.com/science/article/pii/S2352146516304227.

[4] Julio A. Sanguesa et al. "A Review on Electric Vehicles: Technologies and Challenges". In: *Smart Cities* 4.1 (2021), pp. 372–404. DOI: 10.3390/smartcities4010022. URL: https://www.mdpi.com/2624-6511/4/1/22.

[5] Maria Xylia et al. "Impact of bus electrification on carbon emissions: The case of Stockholm". In: *Journal of Cleaner Production* 209 (2019), pp. 74–87. DOI: https://doi.org/10.1016/j.jclepro.2018.10.085. URL: https://www.sciencedirect.com/science/article/pii/S0959652618330993.

[6] M. Bartłomiejczyk et al. *Dynamic Charging of Electric Buses as a Way to Reduce Investment Risks of Urban Transport System Electrification*. www.semanticscholar.org, 2019. URL: https://www.semanticscholar.org/paper/Dynamic-Charging-of-Electric-Buses-as-a-Way-to-of-Bart%5C%C5%5C%82omiejczyk-Po%5C%C5%5C%82om/6ef2448d075df6d8afa9b7ecda039ed2c5c68aa2 (visited on 01/12/2023).

[7] *In-Motion-Charging for emission-free public transport Interim report on the Electric Mobility Europe (EMEurope) project trolley:2.0 two years after project start*. 2020. URL: https://www.electricmobilityeurope.eu/wp-content/uploads/2020/09/Trolley-2-0-Zwischenbericht-english-final.pdf (visited on 01/12/2023).

[8] Fabian Bergk et al. "Potential of In-Motion Charging Buses for the Electrification of Urban Bus Lines". In: *Journal of Earth Sciences and Geotechnical Engineering* 6 (2016), pp. 1792–9660. URL: https://www.scienpress.com/Upload/GEO/Vol%5C%206_4_21.pdf (visited on 01/12/2023).

[9] . *KNOWLEDGE BRIEF*. 2019. URL: https://cms.uitp.org/wp/wp-content/uploads/2021/01/Knowledge-Brief-Infrastructure-May-2019-FINAL.pdf.

[10] Mikolaj Bartlomiejczyk. *The Examples of Dynamic Charging Applications*. Dynamic Charging of Electric Buses, 2020.

[11] Railway-News. *Solingen Public Transport Invests in IMC Buses from Kiepe Electric*. Bus-News, Oct. 2020. URL: https://bus-news.com/solingen-public-transport-invests-in-imc-buses-from-kiepe-electric/ (visited on 02/27/2023).

[12] Les Brunton. "The trolleybus story". In: *IEE Review* 38 (1992), p. 57. DOI: 10.1049/ir:19920024. (Visited on 04/13/2022).

[13] . *KNOWLEDGE BRIEF*. July 2021. URL: https://cms.uitp.org/wp/wp-content/uploads/2021/07/Knowledge-Brief-IMC.pdf.

[14] Ibrahim Diab et al. "An Adaptive Battery Charging Method for the Electrification of Diesel or CNG Buses as In-Motion-Charging Trolleybuses". In: *IEEE Transactions on Transportation Electrification* (2023), pp. 1–1. DOI: 10.1109/tte.2023.3243022. (Visited on 02/11/2023).

[15] Marek Bistřický. “A Valley-Charging Power Approach for the Integration of In-Motion Charging Buses in DC Trolleygrids”. In: *repository.tudelft.nl* (2022). URL: https://repository.tudelft.nl/islandora/object/uuid%3Ab6eddf95-1114-4ae3-8212-b02617a1cc78 (visited on 08/29/2023).

[16] Thomas Nemeth et al. “Lithium titanate oxide battery cells for high-power automotive applications – Electro-thermal properties, aging behavior and cost considerations”. In: *Journal of Energy Storage* 31 (Oct. 2020), p. 101656. DOI: 10.1016/j.est.2020.101656. URL: https://www.sciencedirect.com/science/article/abs/pii/S2352152X20314936 (visited on 03/29/2021).

[17] Heide Budde-Meiwes et al. “A review of current automotive battery technology and future prospects”. In: *Proceedings of the Institution of Mechanical Engineers, Part D: Journal of Automobile Engineering* 227 (Apr. 2013), pp. 761–776. DOI: 10.1177/0954407013485567.

[18] Will Ayers et al. *Comparative Payback of Lithium-Ion Batteries for Pacific NW Ferries*. 2016. (Visited on 01/19/2023).

[19] Matthieu Urbain et al. “Energetical Modeling of Lithium-Ion Batteries Including Electrode Porosity Effects”. In: *IEEE Transactions on Energy Conversion* 25 (Sept. 2010), pp. 862–872. DOI: 10.1109/TEC.2010.2049652. URL: https://ieeexplore.ieee.org/document/5484532 (visited on 01/20/2023).

[20] Martin Winter et al. “Insertion Electrode Materials for Rechargeable Lithium Batteries”. In: *Advanced Materials* 10 (July 1998), pp. 725–763. DOI: 10.1002/(sici)1521-4095(199807)10:10<725::aid-adma725>3.0.co;2-z. (Visited on 03/31/2022).

[21] Marcin Wołek et al. “Transformation of Trolleybus Transport in Poland. Does In-Motion Charging (Technology) Matter?” In: *Sustainability* 12 (Nov. 2020), p. 9744. DOI: 10.3390/su12229744. (Visited on 09/03/2021).

[22] N. Takami et al. “High-power and long-life lithium-ion batteries using lithium titanium oxide anode for automotive and stationary power applications”. In: *Journal of Power Sources* (2013). URL: https://www.semanticscholar.org/paper/High-power-and-long-life-lithium-ion-batteries-for-Takami-Inagaki/2cfe4fa0dae30c6df4cf0759280ec83161798146 (visited on 01/20/2023).

[23] Tsutomu Ohzuku et al. “Zero□Strain Insertion Material of Li□[□Li1□/□3Ti5□/□3□]□□O□4 for Rechargeable Lithium Cells”. In: *Journal of The Electrochemical Society* 142 (May 1995), pp. 1431–1435. DOI: 10.1149/1.2048592. (Visited on 09/10/2020).

[24] Jun Lu et al. “High-Performance Anode Materials for Rechargeable Lithium-Ion Batteries”. In: *Electrochemical Energy Reviews* 1 (Mar. 2018), pp. 35–53. DOI: 10.1007/s41918-018-0001-4.

[25] Wiljan Vermeer et al. “A Comprehensive Review on the Characteristics and Modelling of Lithium-ion Battery Ageing”. In: *IEEE Transactions on Transportation Electrification* (2021), pp. 1–1. DOI: 10.1109/tte.2021.3138357. (Visited on 02/19/2022).

[26] Yemeserach Mekonnen et al. *A review of cathode and anode materials for lithium-ion batteries*. IEEE Xplore, 2016. DOI: 10.1109/SECON.2016.7506639. URL: https://ieeexplore.ieee.org/abstract/document/7506639?casa_token=AoCQLEg8ae8AAAAA:gAIt0KOpIbVYELs3JprXMriFmLeQzsD1k_tWPd9Yvq_1Y1EdviosgSM92hHcUc_HgYHLxE544A (visited on 05/06/2021).

[27] Pallavi Verma et al. “A review of the features and analyses of the solid electrolyte interphase in Li-ion batteries”. In: *Electrochimica Acta* 55 (Sept. 2010), pp. 6332–6341. DOI: 10.1016/j.electacta.2010.05.072. URL: https://www.sciencedirect.com/science/article/pii/S0013468610007747.

[28] Shengshui Zhang et al. “Understanding Solid Electrolyte Interface Film Formation on Graphite Electrodes”. In: *Electrochemical and Solid-State Letters* 4 (2001), A206. URL: https://www.academia.edu/7294920/Understanding_Solid_Electrolyte_Interface_Film_Formation_on_Graphite_Electrodes (visited on 02/27/2023).

[29] Christoph R. Birkl et al. “Degradation diagnostics for lithium ion cells”. In: *Journal of Power Sources* 341 (Feb. 2017), pp. 373–386. DOI: 10.1016/j.jpowsour.2016.12.011. URL: https://www.sciencedirect.com/science/article/pii/S0378775316316998?via%3Dihub.

[30] J. Vetter et al. “Ageing mechanisms in lithium-ion batteries”. In: *Journal of Power Sources* 147 (Sept. 2005), pp. 269–281. DOI: 10.1016/j.jpowsour.2005.01.006. URL: https://www.sciencedirect.com/science/article/abs/pii/S0378775305000832.

[31] Marco Beyeler. *Alterungsoptimierte Batteriebewirtschaftung mithilfe von Open Source Simulation, Fahchhochschule Bern*. Feb. 2022.

[32] Thomas Bank. *Performance and aging analysis of high-power lithium titanate oxide cells for low-voltage vehicl... - RWTH AACHEN UNIVERSITY ISEA - English*. www.isea.rwth-aachen.de, 2021. URL: https://www.isea.rwth-aachen.de/cms/ISEA/Forschung/Publikationen/~ojpu/Details/?file=835197&lidx=1 (visited on 09/19/2023).

[33] Sybrand ten Cate Hoedemaker. “An assessment of the relationship between battery size, charging strategy and battery lifetime”. In: *repository.tudelft.nl* (2017). URL: https://repository.tudelft.nl/islandora/object/uuid%3A81aee798-31bc-4628-82a7-ab03937d1161?collection=education (visited on 09/19/2023).

[34] Yong Tian et al. “Comparison Study on Two Model-Based Adaptive Algorithms for SOC Estimation of Lithium-Ion Batteries in Electric Vehicles”. In: *Energies* 7 (Dec. 2014), pp. 8446–8464. DOI: 10.3390/en7128446. (Visited on 12/30/2019).

[35] Xiaosong Hu et al. “A comparative study of equivalent circuit models for Li-ion batteries”. In: *Journal of Power Sources* 198 (Jan. 2012), pp. 359–367. DOI: 10.1016/j.jpowsour.2011.10.013. URL: https://www.sciencedirect.com/science/article/pii/S0378775311019628 (visited on 10/16/2019).

[36] W.Y. Low et al. “Electrical model to predict current–voltage behaviours of lithium ferro phosphate batteries using a transient response correction method”. In: *Journal of Power Sources* 221 (Jan. 2013), pp. 201–209. DOI: 10.1016/j.jpowsour.2012.07.140. (Visited on 06/15/2022).

[37] Johannes Schmalstieg et al. “A holistic aging model for Li(NiMnCo)O2 based 18650 lithium-ion batteries”. In: *Journal of Power Sources* 257 (July 2014), pp. 325–334. DOI: 10.1016/j.jpowsour.2014.02.012. (Visited on 06/14/2021).

[38] John Wang et al. “Degradation of lithium ion batteries employing graphite negatives and nickel–cobalt–manganese oxide + spinel manganese oxide positives: Part 1, aging mechanisms and life estimation”. In: *Journal of Power Sources* 269 (Dec. 2014), pp. 937–948. DOI: 10.1016/j.jpowsour.2014.07.030. URL: https://www.sciencedirect.com/science/article/pii/S037877531401074X?via%3Dihub (visited on 04/04/2023).

[39] You-Jin Lee et al. “Cycle life modeling and the capacity fading mechanisms in a graphite/LiNi0.6Co0.2Mn0.2O2 cell”. In: *Journal of Applied Electrochemistry* 45 (Mar. 2015), pp. 419–426. DOI: 10.1007/s10800-015-0811-6. (Visited on 04/04/2023).

[40] Bolun Xu et al. “Modeling of Lithium-Ion Battery Degradation for Cell Life Assessment”. In: *IEEE Transactions on Smart Grid* 9 (Mar. 2018), pp. 1131–1140. DOI: 10.1109/tsg.2016.2578950.

[41] Andrea Cordoba-Arenas et al. “Capacity and power fade cycle-life model for plug-in hybrid electric vehicle lithium-ion battery cells containing blended spinel and layered-oxide positive electrodes”. In: *Journal of Power Sources* 278 (Mar. 2015), pp. 473–483. DOI: 10.1016/j.jpowsour.2014.12.047. URL: https://www.sciencedirect.com/science/article/abs/pii/S0378775314020758?via%3Dihub (visited on 12/24/2021).

[42] Joris de Hoog et al. “Combined cycling and calendar capacity fade modeling of a Nickel-Manganese-Cobalt Oxide Cell with real-life profile validation”. In: *Applied Energy* 200 (Aug. 2017), pp. 47–61. DOI: 10.1016/j.apenergy.2017.05.018. (Visited on 08/09/2021).

[43] Md Sazzad Hosen et al. “Electro-aging model development of nickel-manganese-cobalt lithium-ion technology validated with light and heavy-duty real-life profiles”. In: *Journal of Energy Storage* 28 (Apr. 2020), p. 101265. DOI: 10.1016/j.est.2020.101265. (Visited on 12/08/2020).

[44] J. Belt et al. “Calendar and PHEV cycle life aging of high-energy, lithium-ion cells containing blended spinel and layered-oxide cathodes”. In: *Journal of Power Sources* 196 (Dec. 2011), pp. 10213–10221. DOI: 10.1016/j.jpowsour.2011.08.067. (Visited on 04/29/2019).

[45] Yidan Gao et al. “Semi-empirical ageing model development of Traction battery”. In: *odr.chalmers.se* (2023). URL: https://odr.chalmers.se/items/56de9e7f-6144-404f-b49e-5fae723eb17f (visited on 08/28/2023).

[46] M. Mauri et al. *Electro-Thermal Aging Model of Li -Ion Batteries for Vehicle-to-Grid Services*. IEEE Xplore, July 2019. DOI: 10.23919/EETA.2019.8804544. URL: https://ieeexplore.ieee.org/document/8804544.

[47] Maciej Swierczynski et al. “Lifetime Estimation of the Nanophosphate $LiFePO_4$/C Battery Chemistry Used in Fully Electric Vehicles”. In: *IEEE Transactions on Industry Applications* 51 (July 2015), pp. 3453–3461. DOI: 10.1109/tia.2015.2405500. (Visited on 05/25/2022).

[48] M. Schimpe et al. “Comprehensive Modeling of Temperature-Dependent Degradation Mechanisms in Lithium Iron Phosphate Batteries”. In: *Journal of The Electrochemical Society* 165 (2018), A181–A193. DOI: 10.1149/2.1181714jes. (Visited on 12/21/2021).

[49] Martin Petit et al. “Development of an empirical aging model for Li-ion batteries and application to assess the impact of Vehicle-to-Grid strategies on battery lifetime”. In: *Applied Energy* 172 (June 2016), pp. 398–407. DOI: 10.1016/j.apenergy.2016.03.119. (Visited on 12/05/2021).

[50] Noshin Omar et al. “Lithium iron phosphate based battery – Assessment of the aging parameters and development of cycle life model”. In: *Applied Energy* 113 (Jan. 2014), pp. 1575–1585. DOI: 10.1016/j.apenergy.2013.09.003.

[51] Joonam Park et al. “Semi-empirical long-term cycle life model coupled with an electrolyte depletion function for large-format graphite/LiFePO 4 lithium-ion batteries”. In: *Journal of Power Sources* 365 (Oct. 2017), pp. 257–265. DOI: 10.1016/j.jpowsour.2017.08.094. (Visited on 04/27/2023).

[52] Girish Suri et al. “A control-oriented cycle-life model for hybrid electric vehicle lithium-ion batteries”. In: *Energy* 96 (Feb. 2016), pp. 644–653. DOI: 10.1016/j.energy.2015.11.075. (Visited on 04/29/2019).

[53] E. Sarasketa-Zabala et al. “Cycle ageing analysis of a LiFePO4/graphite cell with dynamic model validations: Towards realistic lifetime predictions”. In: *Journal of Power Sources* 275 (Feb. 2015), pp. 573–587. DOI: 10.1016/j.jpowsour.2014.10.153.

[54] Maik Naumann et al. “Analysis and modeling of cycle aging of a commercial LiFePO4/graphite cell”. In: *Journal of Power Sources* 451 (Mar. 2020), p. 227666. DOI: 10.1016/j.jpowsour.2019.227666. (Visited on 07/23/2022).

[55] Mahdi Soltani et al. “Degradation behaviour analysis and end-of-life prediction of lithium titanate oxide batteries”. In: *Journal of Energy Storage* 68 (Sept. 2023), p. 107745. DOI: 10.1016/j.est.2023.107745. URL: https://www.sciencedirect.com/science/article/pii/S2352152X23011428 (visited on 06/08/2023).

[56] Ana-Irina Stroe et al. “Accelerated Lifetime Testing of High Power Lithium Titanate Oxide Batteries”. In: *2018 IEEE Energy Conversion Congress and Exposition (ECCE)* (Sept. 2018). DOI: 10.1109/ecce.2018.8557416. (Visited on 01/28/2020).

[57] Mikołaj Bartłomiejczyk. “Practical application of in motion charging: Trolleybuses service on bus lines”. In: *2017 18th International Scientific Conference on Electric Power Engineering (EPE)*. 2017, pp. 1–6. DOI: 10.1109/EPE.2017.7967239.

[58] I. Diab et al. “Toward a Better Estimation of the Charging Corridor Length of In-Motion-Charging Trolleybuses”. In: *2022 IEEE Transportation Electrification Conference and Expo, ITEC 2022* (2022). DOI: 10.1109/ITEC53557.2022.9814021. URL: https://repository.tudelft.nl/islandora/object/uuid%3A22706412-9966-4295-a445-09a5396ed558 (visited on 01/12/2023).

[59] Mikołaj Bartłomiejczyk et al. *ECONOMIC BENEFITS OF DYNAMIC CHARGING OF ELECTRIC BUSES*. 2020. (Visited on 01/12/2023).

[60] Luisa Alfieri et al. “Optimal battery sizing procedure for hybrid trolley-bus: A real case study”. In: *Electric Power Systems Research* 175 (Oct. 2019), p. 105930. DOI: 10.1016/j.epsr.2019.105930. (Visited on 11/18/2020).

[61] Abhishek Singh Omar et al. “Viability of traction battery for battery-hybrid trolleybus”. In: *EVS32 Symposium* (2019), pp. 1–12.

[62] Martin Petit et al. “Development of an empirical aging model for Li-ion batteries and application to assess the impact of Vehicle-to-Grid strategies on battery lifetime”. In: *Applied Energy* 172 (June 2016), pp. 398–407. DOI: 10.1016/j.apenergy.2016.03.119. (Visited on 12/05/2021).

[63] John Wang et al. “Degradation of lithium ion batteries employing graphite negatives and nickel–cobalt–manganese oxide + spinel manganese oxide positives: Part 1, aging mechanisms and life estimation”. In: *Journal of Power Sources* 269 (Dec. 2014), pp. 937–948. DOI: 10.1016/j.jpowsour.2014.07.030. URL: https://www.sciencedirect.com/science/article/pii/S037877531401074X?via%3Dihub.

[64] Surya Prasad. *Empirical battery degradation modelling similarities, differences and shortcomings of various models*. 2022. URL: http://resolver.tudelft.nl/uuid:d9a1260f-1550-4bdf-be79-03d97632e6e5 (visited on 08/03/2023).

[65] Jingkun Li et al. “Past and Present of LiFePO4: From Fundamental Research to Industrial Applications”. In: *Chem* 5 (Jan. 2019), pp. 3–6. DOI: 10.1016/j.chempr.2018.12.012. URL: https://www.sciencedirect.com/science/article/pii/S2451929418305758.

[66] Mohamed S. E. Houache et al. “On the Current and Future Outlook of Battery Chemistries for Electric Vehicles—Mini Review”. In: *Batteries* 8 (July 2022), p. 70. DOI: 10.3390/batteries8070070.

[67] *Harding Energy | Lithium Ion batteries | Lithium Polymer | Lithium Iron Phosphate*. Harding Energy. URL: https://www.hardingenergy.com/lithium-2/.

[68] Yu Miao et al. “Current Li-Ion Battery Technologies in Electric Vehicles and Opportunities for Advancements”. In: *Energies* 12 (Mar. 2019), p. 1074. DOI: 10.3390/en12061074. URL: https://www.mdpi.com/1996-1073/12/6/1074.

[69] *All About Batteries, Part 12: Lithium Titanate (LTO)*. EE Times, Jan. 2015. URL: https://www.eetimes.com/all-about-batteries-part-12-lithium-titanate-lto/.

[70] Alain Mauger et al. “Olivine Positive Electrodes for Li-Ion Batteries: Status and Perspectives”. In: *Batteries* 4 (Aug. 2018), p. 39. DOI: 10.3390/batteries4030039. (Visited on 05/07/2019).

[71] *Volta Foundation - Battery Report*. www.volta.foundation, 2021. URL: https://www.volta.foundation/annual-battery-report.

[72] BloombergNEF. *Lithium-ion Battery Pack Prices Rise for First Time to an Average of* $151/kWh$. BloombergNEF, Dec. 2022. URL: https://about.bnef.com/blog/lithium-ion-battery-pack-prices-rise-for-first-time-to-an-average-of-151-kwh/.

[73] Fastmarkets.com, 2023. URL: https://www.fastmarkets.com/products/forecasting-analysis/newgen/battery-cost-index (visited on 08/13/2023).

[74] Antti Lajunen. “Lifecycle costs and charging requirements of electric buses with different charging methods”. In: *Journal of Cleaner Production* 172 (Jan. 2018), pp. 56–67. DOI: 10.1016/j.jclepro.2017.10.066. (Visited on 04/01/2020).

A Battery Models

A.1. Stress factors influencing calendar aging

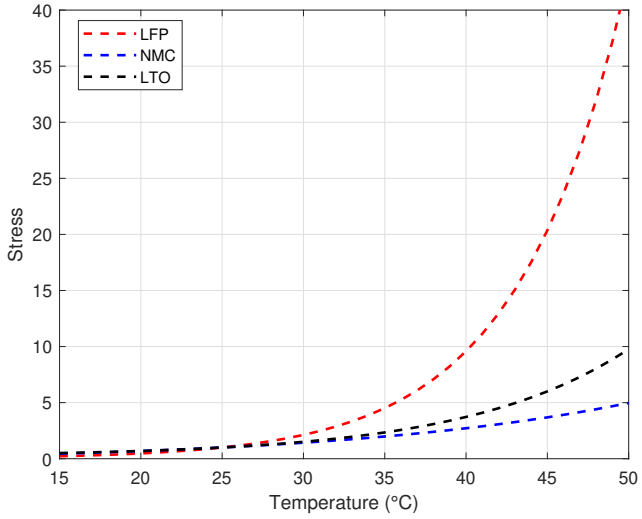

Figure A.1: Stress due to Temperature on Calendar Aging

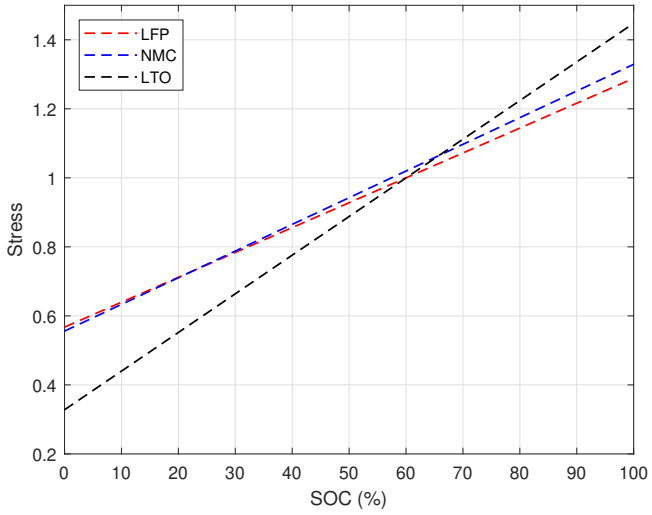

Figure A.2: Stress due to SOC on Calendar Aging

A.2. Stress factors influencing cyclic aging

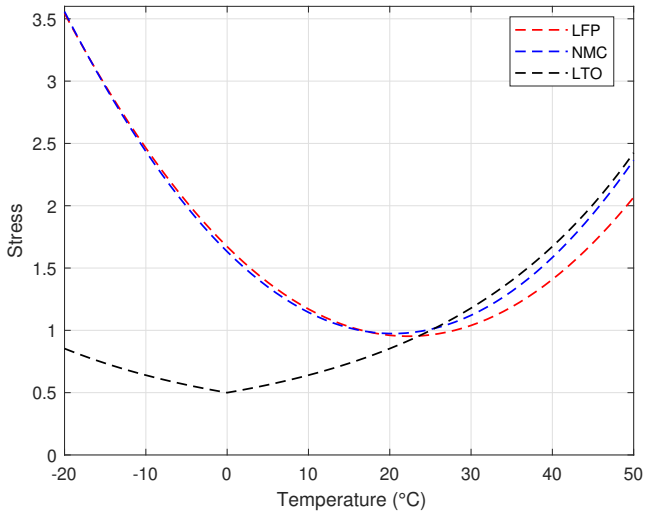

Figure A.3: Stress due to Temperature on Cyclic Aging

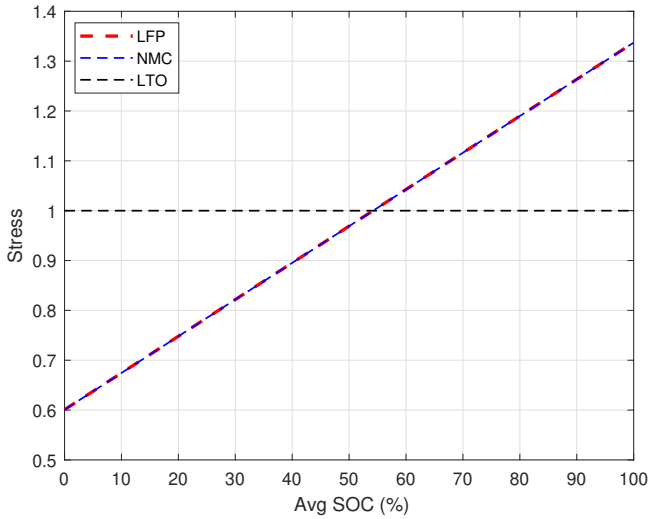

Figure A.4: Stress due to Avg.SOC on Cyclic Aging

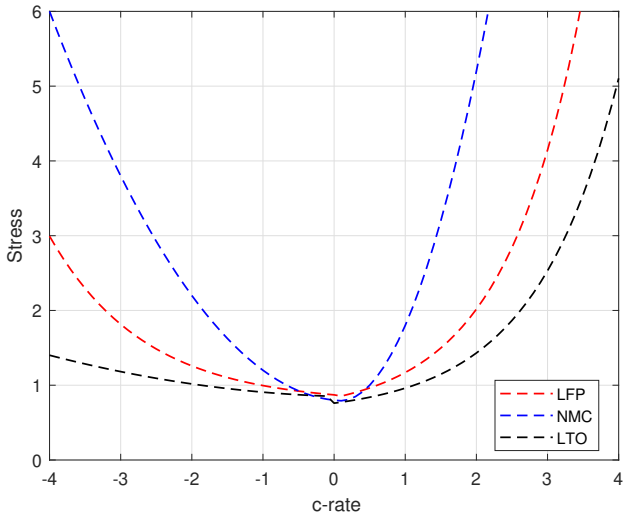

Figure A.5: Stress due to C-rate on Cyclic Aging

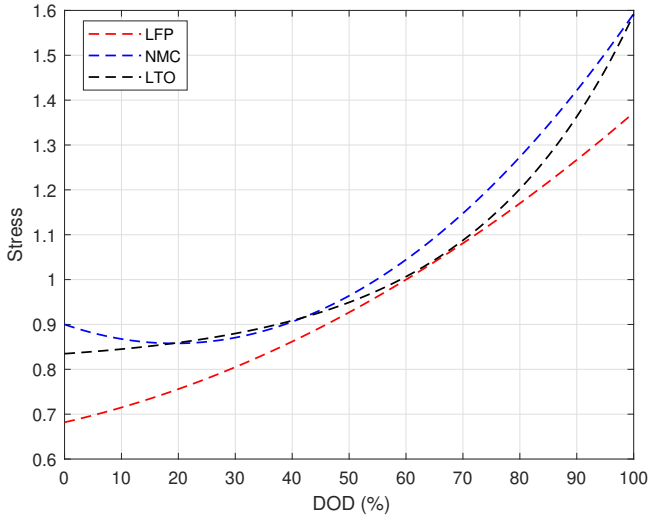

Figure A.6: Stress due to DoD on Cyclic Aging